



# A variational formulation of the quasicontinuum method based on energy sampling in clusters

Bernhard Eidel<sup>a,\*</sup>, Alexander Stukowski<sup>b</sup>

<sup>a</sup> Interdisciplinary Centre for Advanced Materials Simulation (ICAMS), Ruhr-Universität Bochum, Stiepelers Strasse 129, D-44787 Bochum, Germany

<sup>b</sup> Department of Materials Science, TU Darmstadt, Petersenstr. 23, D-64287 Darmstadt, Germany

## ARTICLE INFO

### Article history:

Received 31 October 2007

Accepted 26 September 2008

### Keywords:

Multiscale modeling

Atomistic–continuum bridging

Quasicontinuum

Nanoindentation

Dislocation microstructure

## ABSTRACT

This contribution presents a novel quasicontinuum (QC) approach aiming at a seamless transition from the atomistic to the continuum description of crystalline solids at zero temperature, which heavily draws on the framework proposed by Knap and Ortiz [2001. An analysis of the quasicontinuum method. *J. Mech. Phys. Solids* 49, 1899–1923]. Opposed to Knap and Ortiz, the energy instead of forces is subject to a cluster-based sampling scheme with adaptive resolution. We show that only the present ansatz endows the QC theory with a variational structure leading to conservative forces and symmetric stiffnesses. Equally, we show the strict symmetry in atomic interactions. This approach allows for the direct application of standard minimization methods and guarantees the existence of an equilibrium state provided that the total potential exhibits a minimum. A special focus is on the numerical error in the cluster-based summation rule for energy sampling. We compare two strategies to improve the accuracy, which are also particularly useful to account for surface effects. The fully nonlocal methodology is assessed in nanoindentation into an fcc single crystal. Compared with lattice statics good agreement is achieved with respect to the force–displacement curve, the load level and locus of dislocation nucleation and the dislocation microstructure for a small fraction of the computational costs.

© 2008 Elsevier Ltd. All rights reserved.

## 1. Introduction

The main aim of the present paper is threefold:

(1) First, we propose a novel version of the quasicontinuum (QC) method for zero temperature, which heavily draws on the framework of Knap and Ortiz (2001). We aim to improve it in some notable aspects while maintaining favorable characteristics.

The QC method is an example of a bottom-up, concurrent multiscale method aiming at a seamless link of atomistic with continuum length scales. This aim is achieved by (i) a coarse-graining from fully atomistic resolution via kinematic constraints along with (ii) a sampling of state variables (energy or forces) in coarse-grained regions along with numerical quadrature, where (iii) adaptivity, i.e. spatially adaptive resolution, is governed by a suitable indicator. Properties (i) and (ii) introduce continuum assumptions into the QC method. The first version was proposed by Tadmor et al. (1996a, b) and in a series of papers exemplary problems for multiscale modeling and simulation have been analyzed such as nanoindentation (Phillips et al., 1999; Tadmor et al., 1999; Picu, 2000; Shenoy et al., 2000; Knap and Ortiz, 2001, 2003; Hayes et al., 2005).

\* Corresponding author. Tel.: +49 234 32 29380; fax: +49 234 32 14984.

E-mail address: [bernhard.eidel@ruhr-uni-bochum.de](mailto:bernhard.eidel@ruhr-uni-bochum.de) (B. Eidel).

Furthermore, the simulation of stress-induced phase transformations has been considered in Smith et al. (2000, 2001), the simulation of crack-tip deformation in single crystalline materials by Miller et al. (1998a, b), nanovoid cavitation by Marian et al. (2004), and grain boundaries in Sansoz and Molinari (2005). For an overview of the QC method and applications we refer to Miller and Tadmor (2002). A comparison of QC with other atomistic–continuum coupling methods is presented in Curtin and Miller (2003).

The first version of QC is faced with *ghost forces* defined as spurious forces arising at the boundary between local and nonlocal regions. These forces thus follow from the duality in atomic interactions, where the motion of representative atoms (or rep-atoms) in the local region subject to the Cauchy–Born–Rule (CBR) will effect the energy of nonlocal rep-atoms, while the converse may not be true. A remedy against *ghost forces* is to introduce static correction forces, which exhibit the drawback, that they are not derivable from a ‘correction potential energy’, i.e. they are nonconservative, see Shenoy et al. (1999). This may lead to serious problems with energy conservation during a molecular-dynamics (MD) simulation, as reported in Shimokawa et al. (2004). In order to cure the problem of *ghost forces* without new shortcomings this reference introduces a buffer layer between the two regions of space, where atoms are subject to specific rules, how they interact with their local and nonlocal neighborhood. In a similar spirit is the contribution of E et al. (2006), where the approach of local reconstruction schemes is generalized.

One benefit of the fully-nonlocal QC (QC-FNL) version of Knap and Ortiz (2001) is to overcome the force mismatch between local and nonlocal regions in a most simple and elegant manner by avoiding the CBR and thus to enable the seamless scale transition between fully atomistic resolution and coarse-graining. This means that the scale transition in QC-FNL is realized in a continuous manner by gradual coarse-graining, in QC-CBR it is realized at the discrete interface, where different physical models are in direct neighborhood. In the above structure of QC building blocks, (i)–(iii), QC-FNL introduces for property (ii) the use of summation rules for the sampling of *forces* in spherical clusters in the sense of representative crystallites in order to compute the effective equilibrium equations. Effective means, that instead of minimizing the total energy—as it is done in QC-CBR—a surrogate problem is solved, namely equilibrium of an *approximate force* function. This is based on the fact that energy minimization physically corresponds to solving for the configuration for which the force on each degree of freedom is zero.

At this point the present work elucidates a key new aspect and discusses its consequences; we show that the stiffness matrix derived from the approximate force function in QC-FNL is not symmetric, thus indicating nonconservative forces. This is an unexpected turn, since all forces acting on sampling atoms within the cluster are derived from a well-defined interatomic potential. Based on this analysis we propose a novel QC method that introduces the approximation step of sampling at the energy level instead of the force level, termed QC-eFNL. We show that this ansatz endows the QC-FNL with a variational structure and we discuss its theoretical and numerical advantages. Moreover, we compare the energy-based sampling with the force-based sampling in view of the principle of symmetry in atomic interactions. Furthermore, we discuss for both fully nonlocal QC versions an implication when applying the embedded atom method (EAM).

(II) Second, we present an error analysis which elucidates the quality and assesses the quantity of the error in numerical quadrature within QC-eFNL. The starting point is the observation that the relaxation of a perfect, infinite single-crystal on a nonuniform mesh leads to an inhomogeneous deformation state, where zero displacement is the correct solution. A similar result is reported in E et al. (2006). This example is an important test case in concurrent multiscale modeling, since the exact solution is known a priori. As a consequence, if for the sake of a scale transition an interface is introduced, that couples regions of different physical description, then the corresponding error in terms of spurious relaxation/forces can directly be identified and can be seen as a measure for the departure from a *seamless scale transition*. In QC-CBR, the interface separates local and nonlocal regions and the observed spurious forces are dubbed *ghost forces* as mentioned above. For QC-eFNL we identify the error leading to spurious relaxation as the error in numerical quadrature and discuss two different concepts to control it and finally to reduce it to identically zero. Furthermore, we show by analytical means in a one-dimensional (1D) setting that the exact solution to this particular problem of a homogeneous deformation state can also be obtained, if a *centro symmetry condition* for the mesh is fulfilled, which means that each representative atom, i.e. mesh node, must see an identical environment. It bears emphasis that for a suchlike scenario, i.e. relaxation of an infinite perfect crystal under the additional assumption of homogeneous deformations, Kulkarni et al. (2008) have recently shown that the QC energy equals the exact energy.

(III) Third, we simulate 3D nanoindentation as a benchmark problem for multiscale modeling and simulation in order to assess the main features of QC-eFNL. Nanoindentation is a paradigm for concurrent multiscale methods, since it contains a critical region of confined size, that requires fully atomistic resolution enabling dislocation nucleation and, on the other hand, a coarse-graining for an efficient representation of elastic regions in the crystal. In this setting, the mesh-adaptation abilities controlled by a suitable refinement indicator are crucial to balance efficiency and accuracy of the method. Moreover, for nanoindentation into single crystalline material there is a wealth of investigations applying MD, for ball-indentation into (001) fcc single crystalline material see e.g. Saraev and Miller (2005). It bears emphasis, that nanoindentation is of utmost importance for materials science, since it offers the possibility to understand the fundamental behavior of solids and to extract material properties. For a state-of-the-art review of the recent progress in instrumented indentation we refer to Cheng et al. (2004) and Gouldstone et al. (2007). Experimental results concerning nanoindentation into (001) oriented fcc single crystals are reported in e.g. Gerberich et al. (1996), Rodríguez de la Fuente et al. (2002) and in Minor et al. (2006). In the present work, however, the reference for comparison will be

the results of fully atomistic lattice statics simulation. More specifically, we aim to answer the following questions concerning:

(i) *The efficiency*: How much can the present multiscale framework reduce the computational costs of fully atomistic resolution?

(ii) *The material's global response*: How accurate can QC-eFNL match the material's global response in terms of the characteristic force–depth ( $F$ – $h$ ) curve? The focus here is on the elastic branch up to the event of defect nucleation, marked by a force-drop. As a second indicator we use the accuracy for the resolution of free surface effects. Although this behavior is already reflected by the  $F$ – $h$  curve, it addresses a particular problem of the nonlocal QC method, namely to generally suffer from a significant overestimate of surface effects, see e.g. the review paper of Miller and Tadmor (2002). A rep-atom at the corner of a cubic specimen sees three free surfaces and therefore will be of high-energy. If this considered corner rep-atom is part of a coarse-grained region, it will represent a large volume and therefore its weighting factor in numerical quadrature will be large. The resulting energy will be as though that entire volume of material is located close to free surfaces leading to a considerable overestimate of the energetic contribution of the corner and therefore to spurious relaxation. Thus, to accurately account for surface effects is a challenge within QC simulations. Here, we show that both strategies for error control discussed in this paper are well suited to tackle this problem in nanoindentation.

(iii) *The material's microstructural evolution*: Can QC-eFNL simulations faithfully capture significant details of initial stages of plasticity in terms of the type of evolving dislocation microstructure? Since the energy is not convex, the solution to minimization is highly nonunique, such that many variants of microstructure may evolve beyond the elastic limit. This aspect has been addressed by Knap and Ortiz (2001), where in a 3D simulation of nanoindentation the microstructure for QC differed from lattice statics. Under these adverse circumstances it is an open question, how faithful a concurrent multiscale method can capture microstructures in all details.

According to these aims, the route of the paper is as follows: To put things into perspective we summarize in Section 2 the basic results of lattice statics, since the present QC approach and its precursor of Knap and Ortiz (2001) are direct offsprings of lattice statics, such that a comparison of corresponding force and stiffness expressions will be instrumental. Section 3 summarizes the main features of QC-FNL and ends up in an analysis of the approximate force function by means of the stiffness matrix. Based on this, we present in Section 4 the novel version of QC based on energy sampling and discuss its properties. Section 5 presents an error analysis for QC-eFNL and a comparison QC-FNL and QC-CBR. This leads to the description of different strategies for error control in Section 6. The method is applied in Section 7 to a nanoindentation experiment before we close with a summary in Section 8.

## 2. Basic lattice statics

Considering here the case of one-atomic systems the initial configuration of each atom in a single crystalline material can be identified by its lattice coordinates  $\mathbf{l} = (l^{(1)}, \dots, l^{(d)}) \in \mathbb{Z}^d$ , where  $d$  denotes the dimensions of space. The set  $\mathcal{L} \subset \mathbb{Z}^d$  contains each of the altogether  $N$  atoms in the considered crystal. The spatial initial position  $\mathbf{X}_{\mathbf{l}}$  of an atom with lattice coordinates  $\mathbf{l}$  is defined by

$$\mathbf{X}_{\mathbf{l}} = \sum_{i=1}^d l^{(i)} \mathbf{a}_i, \quad (1)$$

where the basis vectors  $\mathbf{a}_i$  span a simple  $d$ -dimensional Bravais lattice. The displacement vector of the  $\mathbf{l}$ th atom is defined as

$$\mathbf{u}_{\mathbf{l}} = \mathbf{x}_{\mathbf{l}} - \mathbf{X}_{\mathbf{l}}, \quad (2)$$

where  $\mathbf{x}_{\mathbf{l}}$  denotes its current position.

It is assumed that the total potential energy  $E^{\text{tot}}$  of the system can be additively computed as the sum of energies of each atom

$$E^{\text{tot}} = \sum_{\mathbf{k} \in \mathcal{L}} E_{\mathbf{k}}. \quad (3)$$

The particular form of the atomic energy  $E_{\mathbf{k}}$  depends on the model of atomic interactions. In the sequel the atomic energies are computed according to the EAM (Daw and Baskes, 1984). The crucial idea of EAM is that each atom is primarily considered as a foreign atom which must be embedded into the surrounding crystal. This embedding requires a specific amount of energy  $U(\bar{\rho})$  depending on the electron density  $\bar{\rho}$ . The second part in EAM potentials is an ion-ion pair potential term  $V(|\mathbf{r}_{\mathbf{k}\mathbf{l}}|)$ . Under the additional assumption that external forces are derived from a potential  $V^{\text{ext}}$ , the energy of atom  $\mathbf{k}$  follows the general format

$$E_{\mathbf{k}} = U(\bar{\rho}_{\mathbf{k}}) + \frac{1}{2} \sum_{\mathbf{l}} V(|\mathbf{r}_{\mathbf{k}\mathbf{l}}|) + V^{\text{ext}}(\mathbf{x}_{\mathbf{k}}) \quad \text{with} \quad (4)$$

$$\bar{\rho}_{\mathbf{k}} = \sum_{\mathbf{l}} \rho(|\mathbf{r}_{\mathbf{k}\mathbf{l}}|), \quad \mathbf{r}_{\mathbf{k}\mathbf{l}} = \mathbf{x}_{\mathbf{k}} - \mathbf{x}_{\mathbf{l}}. \quad (5)$$

The electron density  $\bar{\rho}_{\mathbf{k}}$  at site  $\mathbf{k}$  is approximated by the superposition of the contributions of all atoms in the neighborhood, given by a new functional  $\rho(r)$ .

Due to applied loads, defects like vacancies, dislocations, grain boundaries, etc. and the effect of free surfaces, the lattice system in its initial geometrical definition generally exhibits a state of nonequilibrium and will relax into an equilibrium configuration, that is a minimizer of the total potential

$$\min E^{\text{tot}}(\{\mathbf{x}_i\}). \quad (6)$$

Since the total energy is not convex, the solution to Eq. (6) is in general nonunique. Therefore, several local minimizers each representing different microstructures exist beyond the elastic limit. From this fundamental mathematical property of  $E^{\text{tot}}$  it is clear, that any slight perturbation of the system—which might stem e.g. from the chosen numerical solution method or from peculiarities in the simulation as the magnitude of stepsize in loading or alike—will affect the local state of equilibrium. This aspect will be recalled in the analysis of the nanoindentation experiment in Section 7.

The force  $\mathbf{f}_{\mathbf{a}}$  acting on atom  $\mathbf{a}$  is the negative derivative of the total potential energy with respect to the atom's current position vector  $\mathbf{x}_{\mathbf{a}}$

$$\begin{aligned} \mathbf{f}_{\mathbf{a}} &= -\frac{\partial E^{\text{tot}}}{\partial \mathbf{x}_{\mathbf{a}}} = -\sum_{\mathbf{k} \in \mathcal{L}} \frac{\partial E_{\mathbf{k}}}{\partial \mathbf{x}_{\mathbf{a}}} \\ &= -\sum_{\mathbf{k} \in \mathcal{L}} \left[ \text{grad } V^{\text{ext}}(\mathbf{x}_{\mathbf{k}}) \frac{\partial \mathbf{x}_{\mathbf{k}}}{\partial \mathbf{x}_{\mathbf{a}}} + \frac{1}{2} \sum_{\mathbf{l} \in \mathcal{L}} V'(|\mathbf{r}_{\mathbf{kl}}|) \frac{\partial |\mathbf{r}_{\mathbf{kl}}|}{\partial \mathbf{x}_{\mathbf{a}}} + U'(\bar{\rho}_{\mathbf{k}}) \frac{\partial \bar{\rho}_{\mathbf{k}}}{\partial \mathbf{x}_{\mathbf{a}}} \right] \\ &= -\text{grad } V^{\text{ext}}(\mathbf{x}_{\mathbf{a}}) - \sum_{\mathbf{l} \in \mathcal{L}} \left[ V'(|\mathbf{r}_{\mathbf{al}}|) \frac{\mathbf{r}_{\mathbf{al}}}{|\mathbf{r}_{\mathbf{al}}|} \right] - \left[ U'(\bar{\rho}_{\mathbf{a}}) \cdot \sum_{\mathbf{l} \in \mathcal{L}} \rho'(|\mathbf{r}_{\mathbf{al}}|) \frac{\mathbf{r}_{\mathbf{al}}}{|\mathbf{r}_{\mathbf{al}}|} \right] - \sum_{\mathbf{k} \in \mathcal{L}} \left[ U'(\bar{\rho}_{\mathbf{k}}) \cdot \rho'(|\mathbf{r}_{\mathbf{ak}}|) \frac{\mathbf{r}_{\mathbf{ak}}}{|\mathbf{r}_{\mathbf{ak}}|} \right], \end{aligned} \quad (7)$$

where  $(\bullet)'$  denotes the derivative of  $(\bullet)$  w.r.t. the function's argument. We use this result as ready reference for a comparison with the force-expressions of two different variants of the QC method.

The second derivative or Hessian of the total energy is called stiffness matrix. It is required in the solution process if the Newton–Raphson method is applied. Furthermore, the stiffness matrix contains information about the state of stability in the crystal. For a system with sufficient displacement boundary conditions, that inhibit rigid body motions, a positive definite matrix  $\mathbf{K}$  indicates a stable state of equilibrium of the lattice. Furthermore, the symmetry of the stiffness matrix indicates, that forces are conservative, i.e. derived from a potential. Equally, its symmetry reflects the symmetry of atomic interactions.

For the subsequent analysis it is sufficient to focus on pair potentials. In this case, force expression Eq. (7)<sub>3</sub> boils down to the first two terms.

The stiffness matrix  $\mathbf{K} \in \mathbb{R}^{Nd \times Nd}$  is composed of submatrices  $\mathbf{k}_{\mathbf{ab}} \in \mathbb{R}^{d \times d}$ . According to the definition, they have for pair potentials the following format

$$\mathbf{k}_{\mathbf{ab}} = \frac{\partial^2 E^{\text{tot}}}{\partial \mathbf{x}_{\mathbf{a}} \partial \mathbf{x}_{\mathbf{b}}} = \frac{\partial}{\partial \mathbf{x}_{\mathbf{b}}} \left( \frac{\partial E^{\text{tot}}}{\partial \mathbf{x}_{\mathbf{a}}} \right) \quad (8)$$

$$\begin{aligned} &= \text{Hess } V^{\text{ext}}(\mathbf{x}_{\mathbf{a}}) \frac{\partial \mathbf{x}_{\mathbf{a}}}{\partial \mathbf{x}_{\mathbf{b}}} + \sum_{\mathbf{l} \in \mathcal{L}} \frac{\partial}{\partial \mathbf{x}_{\mathbf{b}}} \left[ V'(|\mathbf{r}_{\mathbf{al}}|) \frac{\mathbf{r}_{\mathbf{al}}}{|\mathbf{r}_{\mathbf{al}}|} \right] \\ &= \text{Hess } V^{\text{ext}}(\mathbf{x}_{\mathbf{a}}) \delta_{\mathbf{ab}} \mathbf{1} + \sum_{\mathbf{l} \in \mathcal{L}} (\delta_{\mathbf{ab}} - \delta_{\mathbf{lb}}) \left[ \frac{V'(|\mathbf{r}_{\mathbf{al}}|)}{|\mathbf{r}_{\mathbf{al}}|} \mathbf{1} + \left( \frac{V''(|\mathbf{r}_{\mathbf{al}}|)}{|\mathbf{r}_{\mathbf{al}}|^2} - \frac{V'(|\mathbf{r}_{\mathbf{al}}|)}{|\mathbf{r}_{\mathbf{al}}|^3} \right) \mathbf{r}_{\mathbf{al}} \otimes \mathbf{r}_{\mathbf{al}} \right]. \end{aligned} \quad (9)$$

We denote by  $\mathbf{a} \otimes \mathbf{b}$  the tensorial (dyadic) product of two vectors  $\mathbf{a}$  and  $\mathbf{b}$ . Moreover,  $\mathbf{1}$  denotes the  $d \times d$  unity matrix. Eq. (9) can be decomposed into diagonal- and off-diagonal elements

$$\mathbf{k}_{\mathbf{ab}} = -\frac{V'(|\mathbf{r}_{\mathbf{ab}}|)}{|\mathbf{r}_{\mathbf{ab}}|} \mathbf{1} - \left[ \frac{V''(|\mathbf{r}_{\mathbf{ab}}|)}{|\mathbf{r}_{\mathbf{ab}}|^2} - \frac{V'(|\mathbf{r}_{\mathbf{ab}}|)}{|\mathbf{r}_{\mathbf{ab}}|^3} \right] \mathbf{r}_{\mathbf{ab}} \otimes \mathbf{r}_{\mathbf{ab}} \quad \text{for } \mathbf{a} \neq \mathbf{b}, \quad (10)$$

$$\mathbf{k}_{\mathbf{aa}} = \text{Hess } V^{\text{ext}}(\mathbf{x}_{\mathbf{a}}) - \sum_{\mathbf{l} \in \mathcal{L} \setminus \{\mathbf{a}\}} \mathbf{k}_{\mathbf{al}}, \quad (11)$$

where the representation of  $\mathbf{k}_{\mathbf{aa}}$  according to Eq. (11) reflects translational invariance, see e.g. Wallace (1998, Chapter 2).

### 3. Fully nonlocal QC based on force sampling in clusters: QC-FNL

Knap and Ortiz (2001) have proposed a fully nonlocal QC formulation, termed QC-FNL. Conceptually it starts from fully atomistic resolution of lattice statics and introduces two approximations, which can be seen as continuum assumptions. The first is kinematical in nature aiming at a reduction of degrees of freedom by coarse-graining via FE-shape functions, the second applies sampling of forces in clusters of confined size along with summation rules in the spirit of numerical quadrature.

### 3.1. Reduction of the degrees of freedom by kinematic constraints

The reduction of degrees of freedom is accomplished by the introduction of kinematic constraints. Some judiciously selected atoms, called representative atoms or rep-atoms, retain their independent degrees of freedom. They form the set  $\mathcal{L}_h \subseteq \mathcal{L}$ . Following the idea of the finite element method, see e.g. Hughes (2000) and Brenner and Scott (2002), a triangulation of the crystal is performed with representative atoms being mesh nodes. Tetrahedral elements are well suited to fill up a nonregular domain. The nodal displacements are used along with shape functions as kinematic constraints to define a displacement field, all other atoms are forced to follow. The current position  $\mathbf{x}_l$  of a constrained atom  $l \in \overline{\mathcal{L}_h} := \mathcal{L} \setminus \mathcal{L}_h$  is defined according to its initial position  $\mathbf{X}_l$  within an element and the displacements of the corresponding mesh nodes. The most general requirements to the discretization are first, to reduce the number of representative atoms  $N_h = |\mathcal{L}_h|$  such that  $N_h \ll N$ , and second, to ensure high density of rep-atoms up to fully atomistic resolution in regions of interest, where defects nucleate and evolve, like dislocation cores, crack tips among others. To consolidate these two opposite requirements is a trade-off between efficiency and accuracy. The density of representative atoms is controlled by a criterion that measures, how strong the deformations spatially vary. The most simple way to realize the kinematic constraint is via linear finite element shape functions

$$\mathbf{x}_l = \sum_{j \in \mathcal{L}_h} \mathbf{x}_j \varphi_j(\mathbf{X}_l), \quad l \in \overline{\mathcal{L}_h}. \quad (12)$$

The finite element shape functions  $\{\varphi_j\}$  exhibit the properties

$$\sum_{j \in \mathcal{L}_h} \varphi_j(\mathbf{X}_i) = 1 \quad \forall i \in \mathcal{L}, \quad (13)$$

$$\varphi_j(\mathbf{X}_{j'}) = \delta_{jj'} \quad \forall j, j' \in \mathcal{L}_h. \quad (14)$$

According to Eq. (13) shape functions are a partition of unity over  $\mathcal{L}$ , which ensures the exact representation of constant fields. Nodal shape functions  $\varphi_j$  vanish in all elements, where vertex  $j$  is not a mesh node (compact support). This property reduces the sum Eq. (12) to  $d + 1$  terms, which belong to the nodes of the corresponding simplex element of dimension  $d$ . The total potential  $E^{\text{tot}}$ , which depends in lattice statics on each and every atom in the crystal, exhibits less arguments after this coarse-graining or discretization

$$E^{\text{tot}}(\{\mathbf{x}_i | i \in \mathcal{L}\}) \rightarrow E^{\text{tot}}(\{\mathbf{x}_i | i \in \mathcal{L}_h\}) =: E^{\text{tot},h}. \quad (15)$$

Thus, kinematical constraints imply that the search for a minimizer is now restricted to a subspace of the original lattice statics configurational space.

Applying the kinematic constraints Eq. (12) to the distance vector  $\mathbf{r}_{kl}$  between two atoms  $k$  and  $l$ , Eq. (5)<sub>2</sub>, reads

$$\mathbf{r}_{kl} = \mathbf{x}_k - \mathbf{x}_l = \sum_{j \in \mathcal{L}_h} \mathbf{x}_j [\varphi_j(\mathbf{X}_k) - \varphi_j(\mathbf{X}_l)]. \quad (16)$$

Applying Eq. (16) and the derivative of  $\mathbf{r}_{kl}$  with respect to the position vector  $\mathbf{x}_a$ ,  $\mathbf{a} \in \mathcal{L}_h$ , yields the summed-up force acting on the FE-mesh node  $\mathbf{a}$

$$\mathbf{f}_a^h = - \frac{\partial E^{\text{tot},h}}{\partial \mathbf{x}_a} = \sum_{k \in \mathcal{L}} \mathbf{f}_k \varphi_a(\mathbf{X}_k) \quad (17)$$

$$= - \sum_{k \in \mathcal{L}} \left[ \frac{1}{2} \sum_{l \in \mathcal{L}} V'(|\mathbf{r}_{kl}|) \frac{\mathbf{r}_{kl}}{|\mathbf{r}_{kl}|} [\varphi_a(\mathbf{X}_k) - \varphi_a(\mathbf{X}_l)] \right] \quad (18)$$

$$= - \sum_{k \in \mathcal{L}} \left[ \sum_{l \in \mathcal{L}} V'(|\mathbf{r}_{kl}|) \frac{\mathbf{r}_{kl}}{|\mathbf{r}_{kl}|} \right] \varphi_a(\mathbf{X}_k), \quad (19)$$

where the last identity exploits  $\mathbf{r}_{kl} = -\mathbf{r}_{lk}$  and the fact that  $k$  and  $l$  run over  $\mathcal{L}$ . Note that Eq. (17) contains a sum over all atoms  $k \in \mathcal{L}$  and therefore does not gain efficiency compared with the fully atomistic resolution of lattice statics apart from the reduced number of degrees of freedom. It requires an additional approximation concerning the energy or force calculation to reduce the computational burden.

### 3.2. Cluster-based summation rule for forces

Energy minimization physically corresponds to solving for the configuration for which the force on each degree of freedom is zero. This fact suggests, that equilibrium can be sought by directly working from an approximate expression for the forces  $\mathbf{f}_a^h$

$$\mathbf{f}_a^h = \mathbf{0} \quad \forall \mathbf{a} \in \mathcal{L}_h \quad (20)$$

rather than from the explicit differentiation of an energy functional.

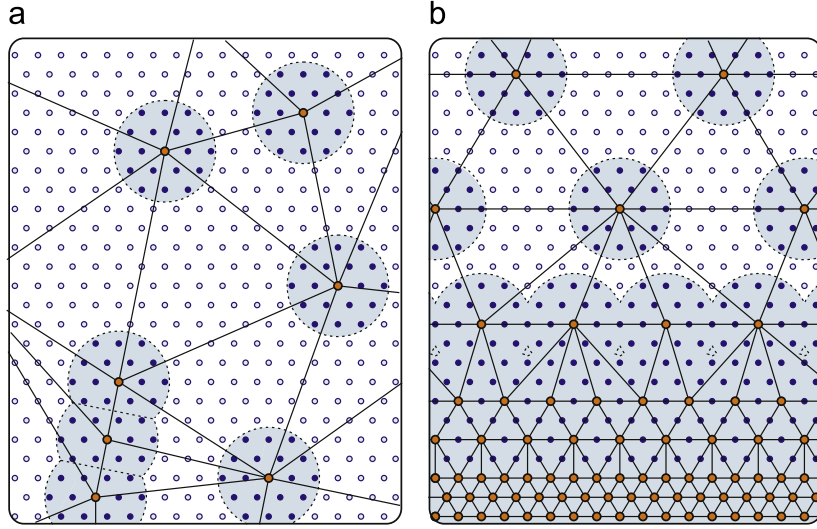


**Fig. 1.** Schematic representation of sampling clusters. Atomic forces are calculated only for atoms within a sphere of radius  $R_c$  around a representative atom. The cluster summation rule Eq. (21) yields the nodal forces. For overlapping clusters, as in (a), the sampling atoms in the intersection are attributed to the nearest representative atom. For exactly the same distance to two or more representative atoms the choice is random. A seamless transition of a coarse-grained region to a region of fully atomistic resolution is illustrated in (b).

Consequently, [Knap and Ortiz \(2001\)](#) apply numerical quadrature for force calculation as the second approximation step of their QC method. Force calculation is no longer performed at each lattice site in the entire crystal but in spherical sampling clusters in the sense of representative crystallites, see [Fig. 1](#). A representative atom is the center of a cluster of radius  $R_c$ , hence cluster  $\mathcal{C}_i$  is defined as  $\mathcal{C}_i = \{\mathbf{k} : |\mathbf{X}_k - \mathbf{X}_i| \leq R_c(\mathbf{i})\}$ . Omitting here and in the sequel the contribution of an external potential  $V^{\text{ext}}$  the cluster summation rule reads, cf. [Knap and Ortiz \(2001, Eq. \(30\)\)](#)

$$\begin{aligned} \mathbf{f}_a^h &= \sum_{\mathbf{i} \in \mathcal{L}_h} n_i \sum_{\mathbf{k} \in \mathcal{C}_i} \mathbf{f}_k \varphi_a(\mathbf{X}_k) \\ &= - \sum_{\mathbf{i} \in \mathcal{L}_h} n_i \sum_{\mathbf{k} \in \mathcal{C}_i} \left[ \sum_{\mathbf{l} \in \mathcal{L}} V'(|\mathbf{r}_{kl}|) \frac{\mathbf{r}_{kl}}{|\mathbf{r}_{kl}|} \right] \varphi_a(\mathbf{X}_k). \end{aligned} \quad (21)$$

The cluster weights  $n_i$ ,  $\mathbf{i} \in \mathcal{L}_h$  are calculated under the requirement, that the summation over all linear interpolation functions must be exact, see [Knap and Ortiz \(2001\)](#). When the clusters shrink to the size of the rep-atoms, i.e.  $\mathcal{C}_i = \{\mathbf{i}\} \forall \mathbf{i} \in \mathcal{L}_h$ , it holds  $\varphi_a(\mathbf{X}_k) = \delta_{ak}$ , and the cluster summation rule boils down to a node-based summation rule  $\mathbf{f}_a^h = \sum_{\mathbf{k} \in \mathcal{L}_h} n_k \mathbf{f}_k \varphi_a(\mathbf{X}_k) = n_a \mathbf{f}_a$ . In this case the weighting factor  $n_k$  is the number of atoms represented by rep-atom  $\mathbf{k}$ , thus  $n_k = \sum_{\mathbf{l} \in \mathcal{L}} \varphi_k(\mathbf{X}_l) \forall \mathbf{k} \in \mathcal{L}_h$ , which implies  $n_k = 1$  for fully atomistic resolution, i.e.  $\mathbf{l} \in \mathcal{L}$ , and which makes sure, that  $\sum_{\mathbf{k} \in \mathcal{L}_h} n_k = |\mathcal{L}|$  is fulfilled.

[Knap and Ortiz \(2001\)](#) report two advantages of the cluster-based summation rule compared with the node-based summation rule. First, the node-based summation leads to a rank-deficiency of the finite element stiffness matrix. Besides the six admissible zero eigenvalues corresponding to rigid body motions there exists an additional zero eigenvalue corresponding to a spurious zero energy mode. This deficiency is overcome by an increased cluster size. The second advantage is that increasing the cluster size improves the accuracy, which implies the feasibility of error estimation. In the present work this property will be exploited for the construction of an effective concept to improve the accuracy, see Section 6.3.

### 3.3. Force sampling implies unsymmetric stiffness matrices

In the sequel we further analyze force expression Eq. (21) via the corresponding stiffness matrix.

The stiffness matrix  $\mathbf{K} \in \mathbb{R}^{N_h d \times N_h d}$  of the static system is composed of the block submatrices  $\mathbf{k}_{ab} \in \mathbb{R}^{d \times d}$ , where the latter are defined according to Eq. (8)<sub>1</sub>. In the approach of [Knap and Ortiz \(2001\)](#) the total potential is not directly at hand, because sampling is performed at the force level. For that reason the calculation of the stiffness matrix must resort to the force expression Eq. (21)

$$\begin{aligned} \mathbf{k}_{ab}^h &= - \frac{\partial \mathbf{f}_a^h}{\partial \mathbf{X}_b} = \sum_{\mathbf{i} \in \mathcal{L}_h} n_i \sum_{\mathbf{k} \in \mathcal{C}_i} - \frac{\partial \mathbf{f}_k}{\partial \mathbf{X}_b} \\ &= \sum_{\mathbf{i} \in \mathcal{L}_h} n_i \sum_{\mathbf{k} \in \mathcal{C}_i} \varphi_a(\mathbf{X}_k) \sum_{\mathbf{l} \in \mathcal{L}} [\varphi_b(\mathbf{X}_k) - \varphi_b(\mathbf{X}_l)] \left[ \frac{V'(|\mathbf{r}_{kl}|)}{|\mathbf{r}_{kl}|} \mathbf{1} + \left( \frac{V''(|\mathbf{r}_{kl}|)}{|\mathbf{r}_{kl}|^2} - \frac{V'(|\mathbf{r}_{kl}|)}{|\mathbf{r}_{kl}|^3} \right) \mathbf{r}_{kl} \otimes \mathbf{r}_{kl} \right]. \end{aligned} \quad (22)$$

The stiffness matrix according to Eq. (22) generally is unsymmetric since the product  $[\varphi_b(\mathbf{X}_k) - \varphi_b(\mathbf{X}_l)]\varphi_a(\mathbf{X}_k)$  is not invariant with respect to an interchange of  $\mathbf{a}$  and  $\mathbf{b}$ . This indicates that the forces according to Eq. (21) are nonconservative and that a corresponding total potential does not exist. This is true, although forces  $\mathbf{f}_k$  acting on sampling atoms are derived from interatomic potentials. If a total potential exists that matches the force expression of Eq. (21) in a variational relation, the stiffness matrix is symmetric due to Eq. (8)<sub>1</sub> and the equality of mixed partial derivatives. The reason is that the approximation step of sampling along with the cluster summation rule is introduced at the force level, which cuts off the variational link between the potential and corresponding forces.

#### 4. The novel ansatz of sampling at the energy level: QC-eFNL

Based on the finding in the previous section, we strive to improve the force-based ansatz of QC-FNL while preserving the beneficial properties to enable a seamless transition between disparate length-scales.

The key aspect is to apply the approximation step of sampling at the energy level instead of the force level.

##### 4.1. Energy sampling leads to conservative forces and symmetric stiffnesses

Applying the cluster summation rule at the energy level yields the approximated total energy  $E^{\text{QC}}$

$$E^{\text{QC}} = \sum_{\mathbf{i} \in \mathcal{L}_h} n_i \sum_{\mathbf{k} \in \mathcal{C}_i} E_k \approx E^{\text{tot},h} \quad (23)$$

with  $E^{\text{tot},h}$  according to Eq. (15). Again, each representative atom  $\mathbf{i} \in \mathcal{L}_h$  is the center of a spherical cluster  $\mathcal{C}_i$  of sampling atoms. For each of them an explicit energy calculation is performed according to interactions within the cut-off radius. The weighting factor  $n_i \geq 1$  of each representative atom  $\mathbf{i}$  represents the contribution of this cluster to the total energy  $E^{\text{QC}}$ .

In search of a state of equilibrium, a local minimizer of the approximated total potential has to be calculated by appropriate numerical means. This task generally requires both, the value of the functional itself and its first derivatives as it is the case for the computationally efficient conjugate gradient (CG) method, see e.g. Luenberger (1989, Chapter 8), or Shewchuk (1994).

Applying Eq. (23) to force calculation at node  $\mathbf{a}$  we get

$$\mathbf{f}_a^h = -\frac{\partial E^{\text{QC}}}{\partial \mathbf{x}_a} = -\sum_{\mathbf{i} \in \mathcal{L}_h} n_i \sum_{\mathbf{k} \in \mathcal{C}_i} \frac{\partial E_k}{\partial \mathbf{x}_a} = -\sum_{\mathbf{i} \in \mathcal{L}_h} n_i \sum_{\mathbf{k} \in \mathcal{C}_i} \frac{1}{2} \sum_{\mathbf{l} \in \mathcal{L}} \left[ V'(|\mathbf{r}_{kl}|) \frac{\mathbf{r}_{kl}}{|\mathbf{r}_{kl}|} [\varphi_a(\mathbf{X}_k) - \varphi_a(\mathbf{X}_l)] \right] \quad (24)$$

and after some algebra we arrive at the stiffness matrix

$$\begin{aligned} \mathbf{k}_{ab}^h &= \frac{\partial^2 E^{\text{QC}}}{\partial \mathbf{x}_a \partial \mathbf{x}_b} \\ &= \sum_{\mathbf{i} \in \mathcal{L}_h} n_i \sum_{\mathbf{k} \in \mathcal{C}_i} \frac{1}{2} \sum_{\mathbf{l} \in \mathcal{L}} [\varphi_a(\mathbf{X}_k) - \varphi_a(\mathbf{X}_l)] [\varphi_b(\mathbf{X}_k) - \varphi_b(\mathbf{X}_l)] \left[ \frac{V'(|\mathbf{r}_{kl}|)}{|\mathbf{r}_{kl}|} \mathbf{1} + \left( \frac{V''(|\mathbf{r}_{kl}|)}{|\mathbf{r}_{kl}|^2} - \frac{V'(|\mathbf{r}_{kl}|)}{|\mathbf{r}_{kl}|^3} \right) \mathbf{r}_{kl} \otimes \mathbf{r}_{kl} \right]. \end{aligned} \quad (25)$$

Since the present QC-eFNL approach starts sampling at the primary level of the potential energy, a consistent derivation leads to forces which are conservative and to corresponding stiffness matrices which are strictly symmetric. For this reason the present ansatz of energy sampling along with cluster summation rules endows the theory with a variational structure.

##### 4.2. Symmetry and asymmetry of atomic interactions across the cluster

Force expression Eq. (24) deserves careful interpretation to enrich it with physical insight and to explain source and consequences of the difference to the nodal force expression Eq. (21) from the force-based QC ansatz. Furthermore, factor 1/2 is at odds with familiar results for forces derived from pair potentials. Nevertheless, it exhibits a similar structure as Eq. (18), but for  $\mathbf{k} \in \mathcal{C}_i \subset \mathcal{L}_h$  a simplification as in Eq. (19) does not apply.

First, we point out the equality of Eqs. (24) and (21), if we restrict to force contributions to  $\mathbf{f}_a^h$  due to the interaction of two atoms,  $\mathbf{k}$  and  $\mathbf{l}$ , when they are both sampling atoms. Next, we consider the atomic interactions of a *sampling atom*  $\mathbf{k}$  with a *nonsampling atom*  $\mathbf{l}$  as illustrated in Fig. 2. It is instrumental to explicitly separate all four force terms for this type of interaction and sticking therein to the lattice statics terms for pair potentials:

(1) Force on atom  $\mathbf{k}$  due to energy contribution of atom  $\mathbf{l}$  to  $E_k$ :

$$\tilde{\mathbf{f}}_k = -\frac{\partial E_{k \leftarrow l}}{\partial \mathbf{x}_k} = -\frac{1}{2} V'(|\mathbf{r}_{kl}|) \frac{\mathbf{r}_{kl}}{|\mathbf{r}_{kl}|}.$$

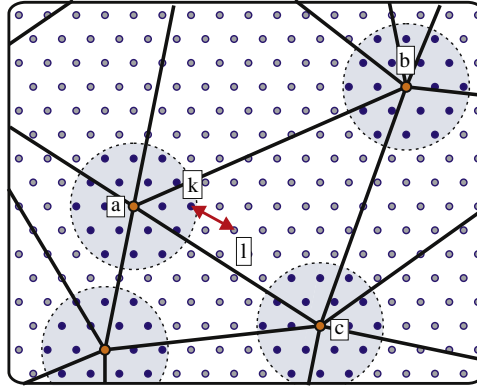


Fig. 2. Illustration of the summation rule for the nodal forces, Eq. (24), within the energy-based ansatz.

(II) Force on atom  $\mathbf{l}$  due to energy contribution of atom  $\mathbf{l}$  to  $E_k$ :

$$\tilde{\mathbf{f}}_{\mathbf{l}} = -\frac{\partial E_{k \leftarrow \mathbf{l}}}{\partial \mathbf{x}_{\mathbf{l}}} = +\frac{1}{2} V'(|\mathbf{r}_{k\mathbf{l}}|) \frac{\mathbf{r}_{k\mathbf{l}}}{|\mathbf{r}_{k\mathbf{l}}|}.$$

(III) Force on atom  $\mathbf{k}$  due to energy contribution of atom  $\mathbf{k}$  to  $E_l$ :

$$\tilde{\mathbf{f}}_{\mathbf{k}} = -\frac{\partial E_{l \leftarrow \mathbf{k}}}{\partial \mathbf{x}_{\mathbf{k}}} = -\frac{1}{2} V'(|\mathbf{r}_{k\mathbf{l}}|) \frac{\mathbf{r}_{k\mathbf{l}}}{|\mathbf{r}_{k\mathbf{l}}|}.$$

(IV) Force on atom  $\mathbf{l}$  due to energy contribution of atom  $\mathbf{k}$  to  $E_l$ :

$$\tilde{\mathbf{f}}_{\mathbf{l}} = -\frac{\partial E_{l \leftarrow \mathbf{k}}}{\partial \mathbf{x}_{\mathbf{l}}} = +\frac{1}{2} V'(|\mathbf{r}_{k\mathbf{l}}|) \frac{\mathbf{r}_{k\mathbf{l}}}{|\mathbf{r}_{k\mathbf{l}}|}.$$

In the sequel we consider force terms captured by energy sampling, afterwards we deal with force sampling. The nonlocal action of energy  $E_{k \leftarrow \mathbf{l}}$  induces a force on atom  $\mathbf{k}$  within the cluster, expression (I), and on atom  $\mathbf{l}$  outside the cluster, expression (II). These two forces are equal up to the opposite sign, Newton's third law holds, *actio = reactio*, which implies symmetric stiffnesses, Eq. (25). The interaction of atom  $\mathbf{k}$  with atom  $\mathbf{l}$  is schematically illustrated in Fig. 2. Both forces are distributed according to their barycentric coordinates from  $\mathbf{k}$  and  $\mathbf{l}$  to adjacent nodes  $\mathbf{a}$ – $\mathbf{c}$ ; for atom  $\mathbf{a}$  the distribution is mediated by factor  $[\varphi_{\mathbf{a}}(\mathbf{X}_{\mathbf{k}}) - \varphi_{\mathbf{a}}(\mathbf{X}_{\mathbf{l}})]$  in Eq. (24). This distribution to adjacent nodes is complete by virtue of Eq. (13). Moreover, since energy sampling is conceptually restricted to clusters, forces at site  $\mathbf{k}$  and site  $\mathbf{l}$  due to the energy contribution  $E_{l \leftarrow \mathbf{k}}$ , expressions (III) and (IV), are missing in Eq. (24); this explains the factor 1/2 therein. It is the function of properly defined weighting factors  $n_i$  to account for the energy contribution of nonsampling atoms. The calculation of  $n_i$  and the rationale behind it is described in Knap and Ortiz (2001).

The application of the force-based ansatz, Eq. (21), gives full account of forces acting on cluster atom  $\mathbf{k}$ , summing up expressions (I) and (III). Contrary to the present ansatz however, Eq. (21) does not consider the opposite force acting on atom  $\mathbf{l}$ , since  $\mathbf{l}$  is not a sampling atom. This lack of symmetry in the interaction of sampling atoms with nonsampling atoms breaks the symmetry of the stiffness matrix, Eq. (22).

In QC-CBR the symmetry in atomic interactions is lost at the interface between local and nonlocal regions, since the motion of rep-atoms in the local region subject to the CBR will effect the energy of nonlocal rep-atoms, while the converse may not be true. This asymmetry is an instance for lacking compatibility which induces ghost forces.

A final remark on the spectral properties of the stiffness matrix Eq. (25) is in order. Computations have shown that the stiffness matrix based on energy sampling exhibits merely the six admissible zero eigenvalues, even for the node-based summation rule. This is in contrast to the already mentioned finding of Knap and Ortiz (2001), where a rank-deficiency of the stiffness matrix derived from force sampling is reported.

#### 4.3. Consequences for the application of EAM-potentials

Next, we focus on EAM-potentials along with the cluster-based summation rule and point out a significant difference between the present, energy-based sampling and the force-based ansatz. Applying an EAM-potential scheme to Eq. (21), we get the nodal force in the force-based sampling approach

$$\mathbf{f}_{\mathbf{a}}^h = -\sum_{\mathbf{i} \in \mathcal{S}_h} n_i \sum_{\mathbf{k} \in \mathcal{C}_i} \varphi_{\mathbf{a}}(\mathbf{X}_{\mathbf{k}}) \left\{ \text{grad } V^{\text{ext}}(\mathbf{x}_{\mathbf{k}}) + \sum_{\mathbf{l} \in \mathcal{S}} \{ V'(|\mathbf{r}_{k\mathbf{l}}|) + [U'(\bar{\rho}_{\mathbf{k}}) + U'(\bar{\rho}_{\mathbf{l}})] \rho'(|\mathbf{r}_{k\mathbf{l}}|) \} \frac{\mathbf{r}_{k\mathbf{l}}}{|\mathbf{r}_{k\mathbf{l}}|} \right\}. \quad (26)$$

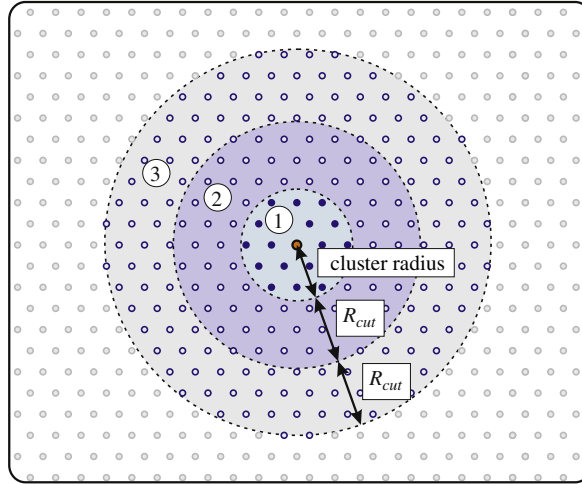


**Fig. 3.** Explanation of Eq. (26): When the forces acting on atoms in region 1 (sampling cluster) are to be calculated, not only the influence of each atom in region 2, i.e. within the range of interaction  $R_{cut}$  must be considered, but additionally the positions of atoms within an extended cut-off radius, that defines region 3.

By contrast, the present energy-based ansatz yields the nodal force

$$\mathbf{f}_a^h = -\frac{\partial E^{QC}}{\partial \mathbf{x}_a} = -\sum_{i \in \mathcal{I}_h} n_i \sum_{\mathbf{k} \in \mathcal{C}_i} \left[ \text{grad } V^{\text{ext}}(\mathbf{x}_k) \varphi_a(\mathbf{X}_k) + \sum_{l \in \mathcal{L}} \left\{ \left[ \frac{V'(|\mathbf{r}_{kl}|)}{2} + U'(\bar{\rho}_k) \rho_l'(|\mathbf{r}_{kl}|) \right] \frac{\mathbf{r}_{kl}}{|\mathbf{r}_{kl}|} [\varphi_a(\mathbf{X}_k) - \varphi_a(\mathbf{X}_l)] \right\} \right]. \quad (27)$$

Note that the electron density  $\bar{\rho}_l$  appears in Eq. (26) but not in Eq. (27). Since index  $l$  represents atoms that interact with sampling atoms  $k$ , nodal force calculation for the force-based sampling requires to evaluate the electron density even for nonsampling atoms, cf. definition of  $\bar{\rho}$  in Eq. (5)<sub>1</sub>. Compared with the energy-based sampling this implies an extra numerical effort, since the position of additional atoms subject to kinematic constraints have to be calculated and corresponding distance vectors have to be considered, see Fig. 3 for an illustration. The energy-based QC approach, however, does not require this extra numerical effort.

## 5. Error analysis

The numerical errors in the QC method compared with lattice statics as its fully atomistic counterpart can be classified as follows:

- (1) Discretization error: only a subset of all atoms are representative atoms, i.e. mesh nodes, that exhibit independent degrees of freedom; the position of all other atoms is determined by the kinematic constraint of interpolation via linear shape functions.
- (2) Error of numerical quadrature:
  - (a) The energy is sampled in clusters of confined size  $\mathcal{C}_i \subset \mathcal{L}$ .
  - (b) Weighting factors are determined such that they are exact, only if the energy is piecewise linear (Knap and Ortiz, 2001).

The discretization error in the present work is reduced by an adaptive refinement strategy based on a heuristic refinement indicator. The construction of a mathematical sound error estimator for the discretization error is beyond the scope of the present paper. Adaptivity is a key feature in concurrent multiscale frameworks and largely determines its efficiency. Here, after each relaxation step a refinement indicator  $\varepsilon(K)$  is calculated for each simplex  $K$  to check the mesh and to detect critical regions, where finer resolution is necessary. If  $\varepsilon(K)$  is larger than a prescribed tolerance  $TOL$ , the element will be refined, otherwise its size is maintained. Here we follow the proposal in Knap and Ortiz (2001) and define this indicator  $\varepsilon(K)$  according to

$$\varepsilon(K) = \sqrt{|\Pi_E(K)|} \cdot h(K)/b, \quad (28)$$

where  $\Pi_E(K)$  is the second invariant of the Green–Lagrange strain tensor  $\mathbf{E}$  in simplex  $K$ , and  $h(K)$  is the size of  $K$ . Since  $b$  denotes the length of the smallest Burgers vector for the given crystal, the criterion, though heuristic, reflects physical reasoning, since the current deformation is compared with the smallest unit of plastic deformation.

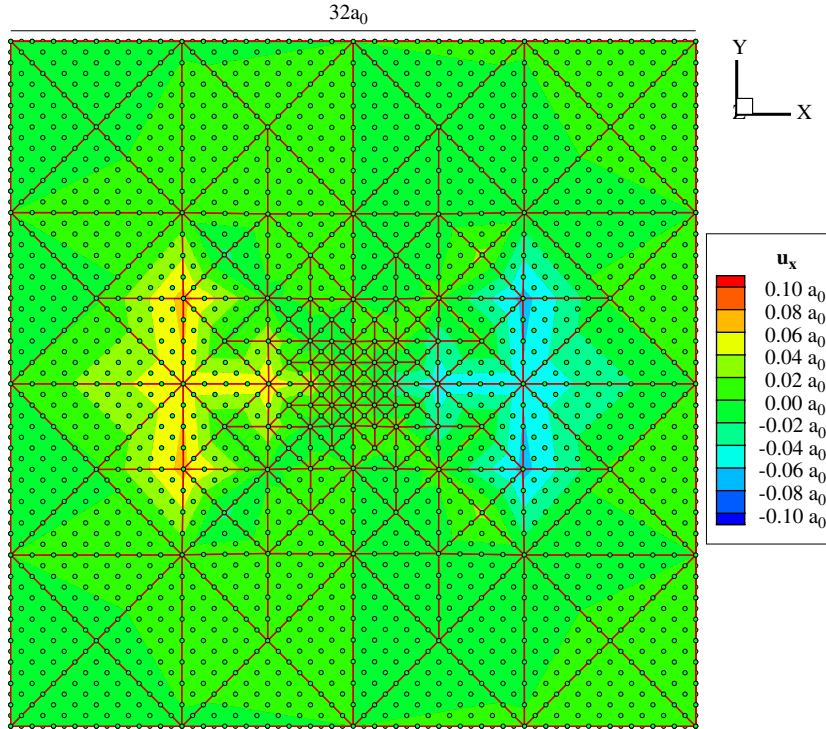


**Fig. 4.** Cross-sectional view into a perfect fcc crystal, (001)-plane, with periodic boundary conditions and fully atomistic resolution in its center. The contour plot of displacement component  $u_x$  after relaxation reveals nonvanishing displacements.

### 5.1. Motivation: relaxation of a perfect infinite crystal on a nonuniform mesh yields an inhomogeneous deformation state

We consider the relaxation of an infinite, perfect fcc single crystal in 3D using periodic boundary conditions and an EAM-potential for Al. Applying QC-eFNL in the calculation on a nonuniform mesh (cluster size  $R_c = 1.0a_0$ ), a somewhat surprising effect is observed. Without applying external forces the crystal exhibits nonzero displacements, see Fig. 4, where the correct solution is zero displacements in the entire crystal. Two references should be mentioned, that consider by analytical means a suchlike perfect crystal for the application of the QC method under different aspects each. For the additional assumption of a homogeneous deformation, Kulkarni et al. (2008) prove that in this scenario the QC energy equals the exact total energy. In this reference the (homogeneous) deformation state thus is part of a priori assumptions, whereas here, the (inhomogeneous) deformation is the result. In a 1D setting of a perfect monatomic chain E et al. (2006) show that forces arise at the interface of regions that exhibit different densities of representative atoms. In that reference these forces are called *ghost forces*.

In the remainder of this section we analyze the source of the observed residual forces in QC-eFNL and discuss their properties compared with the notion of *ghost forces*, which originally are defined as spurious forces at the interface between a local and a nonlocal description, see Miller et al. (1998a) and Shenoy et al. (1999).

### 5.2. Analysis in a 1D model

In order to analyze this effect in a system of reduced complexity, we apply the energy sampling method a 1D crystal for a certain discretization. Suchlike 1D considerations are advantageous since quantities of interest cannot only be calculated by numerical means but are also within analytical reach.

**Example 1.** In the 1D model let the crystal consist of an infinite chain of atoms (set  $\mathcal{L}$ ) with initial spacing  $d$ , which denotes the distance of equilibrium, that minimizes the energy of each atom. The chosen model of atomic interactions in this analysis is the popular Lennard-Jones (LJ) pair-potential (Lennard-Jones, 1924), of the form

$$V(r) = 4\epsilon \left[ \left( \frac{\sigma}{r} \right)^{12} - 2 \left( \frac{\sigma}{r} \right)^6 \right]. \quad (29)$$

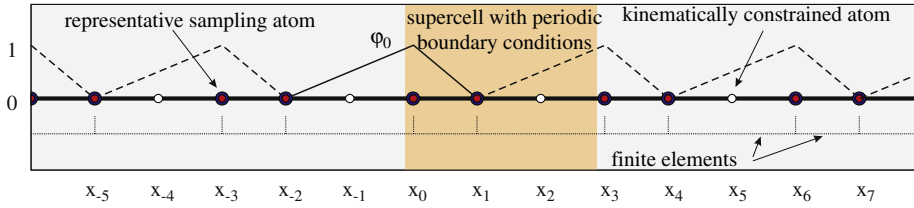


**Fig. 5.** Example 1: Discretization of a one-dimensional atomic chain with periodic boundary conditions. The interpolation function  $\varphi_0$  adjacent to node  $x_0$  is displayed. Red atoms: sampling atoms, white atoms: nonsampling atoms, fat black circles designate representative atoms.

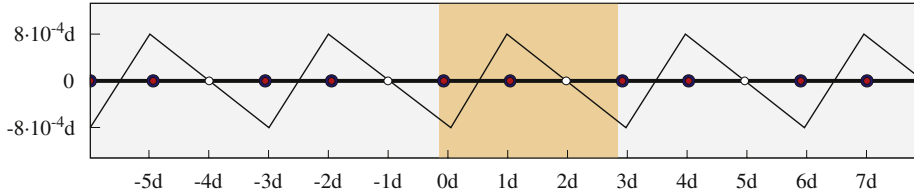


**Fig. 6.** Example 1: Displacements  $u(x)$  in the atomic chain for the minimizer of  $E^{QC}$ .

Herein, parameter  $\varepsilon$  is the well-depth,  $\sigma$  is the separation, at which the interaction force in an infinite chain vanishes. Since interactions exceed the distance to the nearest neighbor, the equilibrium separation  $d$  is not equal with the minimum of  $V(r)$ . For the numerical simulation of the considered infinite system, a *supercell* along with periodic boundary conditions is used. The supercell contains  $N$  atoms and its size is  $N \cdot d$ . The current position vector of an atom during relaxation is denoted by  $x_i$  ( $i = 0 \dots (N - 1)$ ), the initial position vector by  $X_i = i \cdot d$ . The corresponding displacements are defined according to  $u_i = x_i - X_i$ . The set of representative atoms  $\mathcal{L}_h$  and the associated FE-mesh also exhibit the period length  $N \cdot d$ . In the 1D case, each finite element with linear shape functions consists of two representative atoms at its nodal ends. The position of each atom in between the nodes is obtained via interpolation. In the first step of analysis we choose a supercell of size  $N = 3$ , which contains two representative atoms ( $x_0$  and  $x_1$ ) and a kinematically constrained atom ( $x_2$ ). The corresponding FE-mesh is displayed in Fig. 5. This system exhibits two degrees of freedom. Note that the mesh is not symmetric with respect to each representative atom.

The total potential of the supercell for QC-eFNL with node-based summation according to Eq. (23) yields:

$$E^{QC} = \sum_{k \in \mathcal{L}_h} n_k E_k = \sum_{k=0,1} \frac{n_k}{2} \sum_{l \in \mathcal{L}} V(|x_k - x_l|). \quad (30)$$

Minimizing the total energy with respect to the two degrees of freedom ends up in the inhomogeneous deformation state displayed in Fig. 6. Both representative atoms move aside for a small amount breaking the initial periodicity of the crystal. Let us note that if the same system is calculated by means of three representative atoms, Eq. (30) coincides with the fully atomistic lattice statics energy, Eq. (3), and every atom rests at its initial position, since the initial configuration already represents an energetic minimum.

Now we draw our attention to the aforementioned case: each representative atom of the present supercell represents itself and one half of the remaining, kinematically constrained atom. For that reason  $n_k = 1.5$  holds for all  $k \in \mathcal{L}_h$ . Since both rep-atoms have an identical environment, it is sufficient to analyze the behavior of only one of them.

Starting from the initial configuration before relaxation, a variation of the nodal position  $x_0$  of the first representative atom keeping the second  $x_1$  fixed ( $u_1^h = 0$ ) results in an energy behavior displayed in Fig. 7. Since the initial state obviously does not represent the energetic minimum, the nodal forces consequently do not vanish. This behavior can also be studied in terms of the force formula Eq. (24); for the considered system it has the format

$$f_0^h = - \frac{\partial E^{QC}}{\partial x_0} = - \sum_{k=0,1} \frac{3}{4} \sum_{l=-\infty}^{+\infty} V'(|x_k - x_l|) \frac{x_k - x_l}{|x_k - x_l|} [\varphi_0(x_k) - \varphi_0(x_l)].$$

Exploiting  $x_i = X_i = i \cdot d$  for the initial state and  $\varphi_0(x)$  as displayed in Fig. 5, the above equation can be transformed to

$$\begin{aligned} \left. \frac{\partial E^{QC}}{\partial x_0} \right|_{x_0=0} &= \frac{3}{4} \sum_{k=0,1} \sum_{l=-\infty}^{+\infty} V'(|k-l|d) \frac{k-l}{|k-l|} [\varphi_0(kd) - \varphi_0(ld)] \\ &= \frac{3}{4} \sum_{k=0,1} \left[ \underbrace{\sum_{l=-\infty}^{+\infty} V'(|k-l|d) \frac{k-l}{|k-l|} \varphi_0(kd)}_{=0} - \sum_{l=-\infty}^{+\infty} V'(|k-l|d) \frac{k-l}{|k-l|} \varphi_0(ld) \right] \end{aligned}$$

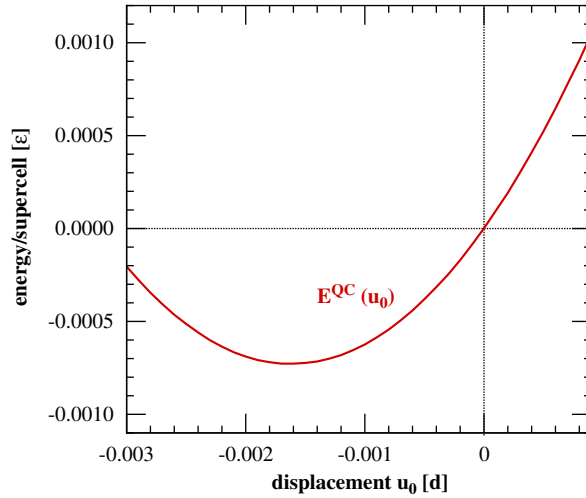


**Fig. 7.** Total energy change in terms of the displacement of the first degree of freedom. The energy of the real ground state for  $u_0^h = 0$  is exactly captured, but the energy function  $E^{\text{QC}}$  exhibits a different minimum below the ground state of the energy.

$$\begin{aligned}
 &= \frac{3}{4} \sum_{k=0;1} \sum_{l=-\infty}^{+\infty} V'(|l|d) \frac{l}{|l|} \varphi_0((k+l)d) \\
 &= \frac{3}{4} \sum_{l=-\infty}^{+\infty} V'(|l|d) \frac{l}{|l|} [\varphi_0(ld) + \varphi_0((l+1)d)].
 \end{aligned} \tag{31}$$

Obviously, the sum in Eq. (31)<sub>4</sub> vanishes for arbitrary potentials  $V$ , only if the term  $[\varphi_0(ld) + \varphi_0((l+1)d)]$  is identical for  $l$  and  $-l$ . This is a symmetry condition for each rep-atom, which does not hold in general. In other words, it requires that each rep-atom sees an identical environment in each direction which is a centro symmetry condition and can be fulfilled by a uniform mesh.

For this specific system it has been shown that the initial state of equidistant atoms is not a state of equilibrium, when the exact energy  $E^{\text{tot}}$  is replaced by the approximated energy  $E^{\text{QC}}$ , cf. Eq. (15). The approximated energy obviously exhibits a different minimum than the exact energy. This fact is remarkable since in this example the approximated energy value matches the true energy exactly in the undeformed state, see Fig. 7.

### 5.3. Residual forces compared with ghost forces

The findings in Example 1 in terms of the spurious relaxation due to residual forces give insight into their source, their characteristics and finally suggest remedies to control them. So this example is an appropriate point of departure to elaborate these properties in comparison with *spurious forces* in the first version of the QC method (Tadmor et al., 1996b). In order to avoid confusion we distinguish by name between *residual forces* in the present QC-formulation (QC-eFNL) and *ghost forces* in QC-CBR. It will turn out to be justified and necessary in view of some remarkable differences.

First, from a phenomenological point of view the observed forces have a similar effect as spurious forces in QC-CBR. Sticking to Example 1, they both lower the energy compared with the exact solution. But already on the phenomenological level of their effects a first difference can be observed; ghost forces in QC-CBR are confined to the local/nonlocal interface, residual forces in QC-eFNL are distributed. This reflects that the scale transition in QC-CBR is realized at discrete interfaces of confined size, in the fully nonlocal QC versions, QC-FNL and the present QC-eFNL, it is realized in a continuous manner by gradual coarse-graining.

Ghost forces in QC-CBR have been thoroughly analyzed and different concepts have been investigated to lower them (Shenoy et al., 1999; Miller and Tadmor, 2002; Curtin and Miller, 2003) and even to avoid them (Shimokawa et al., 2004; E et al., 2006). In QC-CBR the motion of rep-atoms in the local region subject to CBR will effect the energy of nonlocal rep-atoms, while the converse may not be true. Hence, it is this asymmetry in atomic interactions which defines *ghost forces* as spurious forces at the interface between these regions (Shenoy et al., 1999). Briefly, they arise due to different propositions on how atoms interact, which is a lack of compatibility and can be classified as a modeling error.

The fully nonlocal quasicontinuum version of Knap and Ortiz (2001) (QC-FNL) avoids the CBR by sticking to a unified, fully nonlocal description of atomic interactions and therefore a priori overcomes *ghost forces* in the above sense in that it avoids discrete interfaces. Since QC-FNL employs summation rules at the level of forces, it is free from spurious forces and free from corresponding relaxation in the case of the perfect infinite crystal.

Applying energy sampling in the fully nonlocal QC as advocated in the present paper yields residual forces in a distributed manner, if the above requirement of centro symmetry is violated, i.e. if there is a gradient in the discretization.

If the infinite crystal is discretized by a uniform mesh, no matter of the element size, residual forces are identically zero for QC-eFNL. As we will show right below and prove by numerical means in Section 6, residual forces also can be reduced to identically zero on a nonuniform mesh as it is displayed in Fig. 4.

The perfect infinite crystal is an important and popular test case, since it is most simple and the exact solution is known a priori. As a consequence, spurious forces, distributed or confined, directly can be identified and measured as the deviation from a seamless scale transition. However, the result of this test case should not lead to generalizations or misinterpretations; the first caveat is that apart from this example spurious forces will also be present in QC-FNL in general, since they are an error indicator for numerical quadrature, cf. Knap and Ortiz (2001, Section 4.2). In mechanical settings different from the infinite crystal these forces remain hidden, but become apparent if—in a second calculation—a larger cluster size is chosen for comparison. The same is true for QC-eFNL, as will be shown below.

The result of QC-eFNL in this test case might be misleading, if the choice of a uniform mesh to suppress spurious forces suggests that spurious forces generally stem from a kind of a discretization error.

In contrast, they merely arise due to the approximation of the total energy for a fixed mesh,  $E^{\text{tot},h}$ , by its QC counterpart  $E^{\text{QC}}$ , Eq. (23). Consequently, these forces obey the format

$$\mathbf{f}^* = -\text{grad}\{E^{\text{QC}} - E^{\text{tot},h}\}, \quad (32)$$

where the energy error is transformed to a force residual via the grad-operator. This means that residual forces in QC-eFNL stem from the error in numerical quadrature, i.e. cluster-based summation rules, cf. Eq. (23).

As a consequence, QC-eFNL conceptually enables the free choice of the level of accuracy for  $E^{\text{QC}}$  by means of the chosen cluster size, which clearly will be a trade-off between accuracy and numerical costs. In the limiting case of  $E^{\text{QC}} \rightarrow E^{\text{tot},h}$ , where each and every atom is covered by a sampling cluster, the error in numerical quadrature identically vanishes and thus residual forces vanish as well, see Example 3 below.

Eq. (32) also alludes to the inherent property of QC-eFNL to estimate the error in numerical quadrature, simply by calculating the energy twice, but each time applying a different cluster size. This fact will be exploited in Section 6, where different concepts for error reduction are discussed.

Moreover, Eq. (32) reveals that residual forces in QC-eFNL are conservative in nature, they can be derived from a unified total potential and as a consequence, they are symmetric. Ghost forces in QC-CBR are not conservative, since they do not derive from a unified potential and consequently, they are not symmetrical, i.e. the motion of rep-atoms in the local region subject to CBR will effect the energy of nonlocal rep-atoms, while the converse may not be true (Shenoy et al., 1999; Miller and Tadmor, 2002; Curtin and Miller, 2003).

Summarizing, residual forces in QC-eFNL indicate a type of error, that is numerical and—opposed to *ghost forces*—not a consequence of inconsistencies in physical modeling, i.e. inconsistent a priori assumptions on how atoms interact. For that reason, the problem of unphysical forces equally exists in other concurrent multiscale methods coupling different levels of physical accuracy and has already been reported in Kohlhoff et al. (1991) and even in the early work of Mullins and Dokainish (1982).

## 6. How to reduce the numerical error

In the sequel we focus on the error due to the cluster summation rule only. Three different concepts are discussed, that aim to reduce this numerical error:

- (i) Increasing the cluster size.
- (ii) Introducing a correction force field calculated by means of Eq. (32).
- (iii) Combining schemes (i) and (ii) for a novel, hybrid method.

### 6.1. Increasing the number of sampling atoms

The first concept aims to improve the energy approximation by increasing the number of sampling atoms. This concept proposed and assessed by Knap and Ortiz (2001) improves the approximation while keeping the number of representative atoms fixed. For that reason the additional numerical effort arises due to the energy calculation for additional sampling atoms. Fig. 8 exemplary illustrates the effect of additional sampling atoms onto the erroneous displacements in the atomic chain. The chosen discretization is realistic for QC in that it has a local region of interest with an increasing coarse-graining away from it. Obviously, an increase in the cluster size decreases the error for the cost of an additional computation effort. This effort is approximately proportional to the number of sampling atoms  $N_h$  and consequently scales cubic with the cluster size in three dimensions.

### 6.2. Introduction of static correction forces

The second concept is to directly apply static correction forces to reduce the residual forces. A quite similar method was chosen in QC-CBR in order to correct *ghost forces*, see Shenoy et al. (1999). The underlying rationale for calculating static

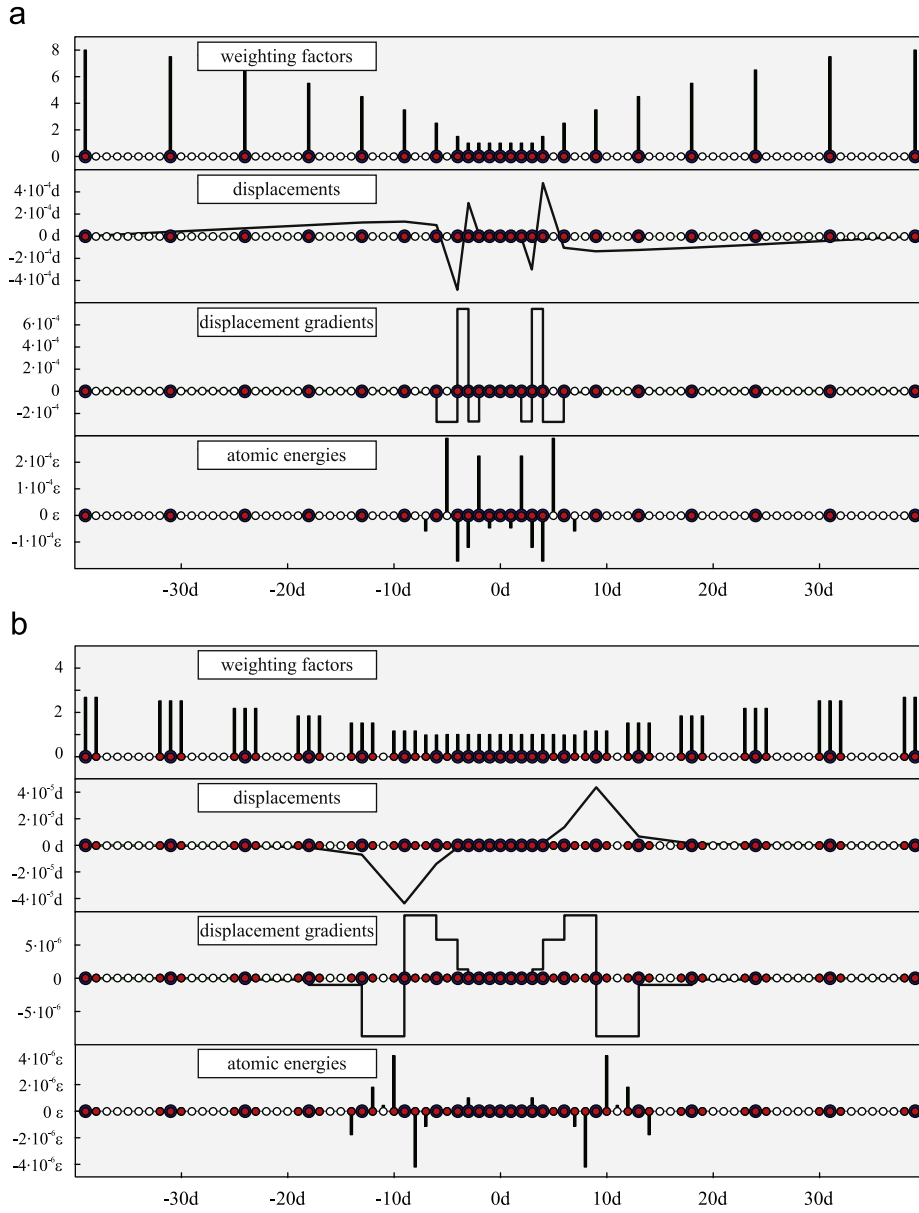


**Fig. 8.** Example 2: Influence of the cluster size  $R_c$  onto the state variables in a perfect single crystal after relaxation. The total system contains 78 atoms with periodic boundary conditions. The central region exhibits fully atomistic resolution and the outer regions are increasingly coarse-grained forming altogether a realistic scenario for typical QC simulations. The initial ground state with equidistant atomic positions is changing during relaxation due to a shift of the minimum of the approximated total energy. The diagrams display weighting factors  $n_k$ , displacements  $u(X)$ , displacement gradients  $\text{grad } u(X)$  and atomic energies  $E_k$  of the relaxed crystal. Inserting additional sampling atoms (red), (a)→(b), reduces the numerical error in terms of the spurious displacements more than one order of magnitude. (a) Cluster radius  $R_c = 0$  atomic distance. (b) Cluster radius  $R_c = 1$  atomic distance.

corrective forces in this reference is to demand that forces acting on any atom be computed using only the formulation which corresponds to its status, a local status or a nonlocal status in the transition zone.

In the context of the present work the residual forces are calculated once at the beginning of the simulation for all nodes in the undeformed state and corresponding static correction forces are applied to the nodes. These correction forces are kept constant during relaxation. Formally, this measurement calculates a corrected potential  $E_c^{\text{QC}}$  by adding a constant force field to  $E^{\text{QC}}$ :

$$E_c^{\text{QC}} = E^{\text{QC}} - \mathbf{f}_0^{h*} \cdot \mathbf{u}^h \quad \text{where } \mathbf{f}_0^{h*} = \text{grad} \{E^{\text{QC}} - E^{\text{tot},h}\}_{|\mathbf{u}^h=0}. \quad (33)$$

This strategy ensures, that  $\text{grad } E_c^{\text{QC}}(\mathbf{u}^h = \mathbf{0}) = \text{grad } E^{\text{tot},h}(\mathbf{u}^h = \mathbf{0})$  holds. The correction via constant force terms is schematically displayed in Fig. 9. A drawback arises following this strategy. It requires once the calculation of the exact

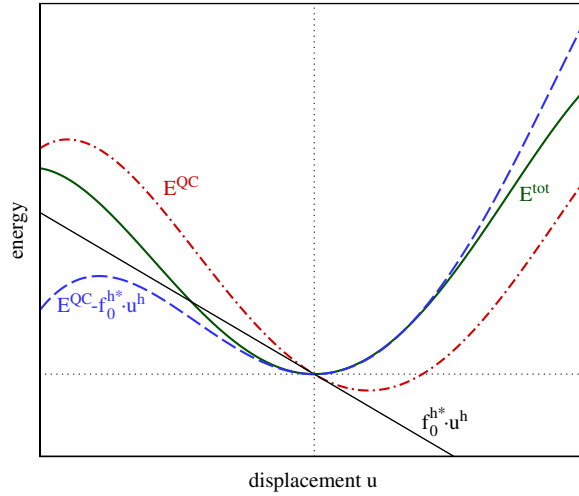


**Fig. 9.** Schematic illustration for the correction of residual forces by applying a static force field.  $E^{\text{QC}}$  approximates the exact energy  $E^{\text{tot}}$ . The minimum of  $E^{\text{QC}}$  deviates from the true minimum of  $E^{\text{tot}}$  by a small shift. Subtracting the energy contribution of correction forces  $f_0^{h*}$  modifies the potential such that both minima coincide.

energy of the system for a given mesh at the simulation start. This may require a prohibitive numerical effort, since the QC method generally aims to simulate very large systems comprising a huge number of atoms, which is the very reason for energy sampling in clusters of confined size. Note that the correction potential  $-f_0^{h*} \cdot u^h$  has the undesired effect of deteriorating the energy function far from the initial state, see Fig. 9. This may induce an undesired shift of the minima in some cases.

### 6.3. Putting it together—a hybrid correction strategy

Each of the two concepts inherently is accompanied by specific drawbacks. A promising method is proposed, that combines both concepts in order to reduce the numerically induced residual forces to an acceptable error bound at moderate costs. The main idea is to calculate the static correction forces not exactly but to approximate them. This requires two energy calculation before relaxation.

- (1) Calculate  $E^{\text{QC}}$  with cluster size  $R_c$  for the initial configuration.
- (2) Calculate for the same configuration  $E^{\text{QC}*}$  with improved accuracy by means of an increased cluster size,  $R_c^* > R_c$ , which also requires a second calculation of weighting factors.
- (3) The gradient of the energy difference with respect to the current nodal position vector at the beginning of a loading/time step renders an estimate of the residual forces. Corresponding static correction forces are applied for the ensuing relaxation process.

Thus we have replaced in Eq. (33)  $E^{\text{tot},h}$  by  $E^{\text{QC}*}$  leading to

$$E_c^{\text{QC}} = E^{\text{QC}} - f_0^{h*} \cdot u^h \quad \text{where } f_0^{h*} = \text{grad} \{E^{\text{QC}} - E^{\text{QC}*}\}|_{u^h=0}. \quad (34)$$

**Example 3.** In order to assess the efficiency of this hybrid approach and the concept of increasing the number of sampling atoms, we design a simple 3D test problem. It consists of an fcc single crystal entailing  $32 \times 32 \times 32$  Bravais-lattice cells with periodic boundary conditions, in order to avoid surface effects. The exact solution to this problem is zero displacements in the entire crystal. It can simply be obtained by means of a uniform mesh, independent of the element size, since this discretization fulfills the mesh centro symmetry condition as elaborated in Example 1. In order to check the scale transition via continuous coarse-graining, we use a nonuniform distribution of representative atoms, which is the same as in Fig. 4. Again, an EAM potential for Al is applied. For the definition of an appropriate error measure we choose the displacements as the quantity of interest. Consequently, the error measure is defined as the root mean square of nodal displacements:

$$\varepsilon_{\text{RMS}} = \sqrt{\frac{1}{N} \sum_i^N \mathbf{u}_i^2}. \quad (35)$$

Table 1 summarizes the results of the calculations on a nonuniform mesh. Increasing the cluster size reduces the error and for  $R_c \geq 4a_0$  the error identically vanishes, which is also reflected by the very short computation time; note that the

**Table 1**

Efficiency of different strategies for error control; lines 1–5: increasing the cluster size, lines 6–9: applying the hybrid correction method

Cluster size for $E^{\text{QC}}$ $R_c [a_0]$	Atoms	Cluster size for $E^{\text{QC}*}$ $R_c^* [a_0]$	Error $\varepsilon_{\text{RMS}} [a_0]$	Computation time $\Delta t$ (s)
0	1	–	$1.5 \times 10^{-1}$	14
$1/\sqrt{2}$	13	–	$2.0 \times 10^{-2}$	29
$2/\sqrt{2}$	55	–	$6.5 \times 10^{-3}$	70
$4/\sqrt{2}$	381	–	$2.1 \times 10^{-3}$	180
4	1061	–	$\equiv 0$	1
0	1	$1/\sqrt{2}$	$2.7 \times 10^{-2}$	17
0	1	$2/\sqrt{2}$	$8.8 \times 10^{-3}$	14
0	1	$4/\sqrt{2}$	$2.9 \times 10^{-3}$	10
0	1	4	$\equiv 0$	3

For  $R_c = 0 [a_0]$  the cluster contains only the rep-atom.

relaxation starts in the configuration which is already the exact solution. In the case  $R_c \geq 4a_0$  each and every atom is covered by a cluster and therefore  $E^{\text{QC}} = E^{\text{tot},h}$  holds, cf. Eq. (23). Hence, it is merely the error in numerical quadrature which causes the observed spurious forces and the numerical origin suggests to reflect this by the name *residual forces* rather than *ghost forces*.

The hybrid correction strategy exhibits the same convergence as the strategy applying constantly a large number of sampling atoms and reduces the error to identically zero for  $R_c^* \geq 4a_0$ . The reason for the remarkable decrease in computation time for increasing the cluster size  $R_c^*$  is that less iterations are necessary. The savings in computation time compared with the variant of a constantly large cluster size is due to the fact that the expensive calculation of  $E^{\text{QC}*}$  is performed only once for a loading step and during CG iterations the recalculation is restricted to  $E^{\text{QC}}$ , which is relatively cheap. Of course, the hybrid correction strategy is not restricted to the calculation of initial relaxations, but equally applicable in the general case, where in Eq. (34)  $\mathbf{u}^h = \mathbf{0}$  is replaced by any  $\mathbf{u}^h$  at the beginning of a loading step.

A final remark is in order to put the error analysis into perspective. The QC method as well as different concurrent multiscale methods are designed to cope with localized deformations or even with some singular sets in solid mechanics like dislocation nucleation, crack growth, grain boundaries and alike. The common property of all these phenomena is that they are confined to small regions with large gradients in the deformation and that these regions are embedded in environments with slowly varying deformations. Hence, it is the stark contrast to homogeneous deformation states (as the correct solution for the perfect infinite single crystal), where concurrent multiscale methods are typically applied by virtue of their atomic coarse-graining with adaptive resolution. The analysis of the observed spurious forces, their different sources as well as concepts to estimate and control them is fundamental for the sound development of numerical methods. As such, this analysis serves to foster concurrent multiscale frameworks in its goal to capture significant physical effects with high fidelity for reduced numerical costs. In this endeavor QC-CBR as well as QC-FNL have proven their predictive capacity in numerous different applications in solid mechanics and materials science, see the references in Section 1. In the same spirit is the analysis of QC-eFNL in the next section.

## 7. Nanoindentation

### 7.1. Problem statement

We choose nanoindentation as a paradigmatic problem for concurrent multiscale methods to showcase the characteristics of the proposed QC-eFNL method and to validate it by comparison with lattice statics. In this assessment three criteria are of cardinal importance:

- (1) *Efficiency*. How much can the present multiscale framework reduce the computational costs?
- (2) *Material's global response*. How accurate does QC-eFNL match the material's global response in terms of the characteristic  $F$ - $h$  curve in its elastic branch up to the event of defect nucleation? How accurate can the effect of free surfaces be resolved?
- (3) *Material's microstructural evolution*. Can QC-eFNL simulations faithfully capture significant details of initial stages of plasticity in terms of the type of evolving dislocation microstructure?

The material under consideration is fcc single crystalline aluminum. The computational box adopted in the computations comprises  $64 \times 64 \times 64$  Bravais-lattice cells. Atoms on the lateral faces of the box are fixed in normal direction to the faces, atoms at the bottom are fixed in  $z$ -direction but free to move within the bottom plane. In Fig. 10 the axes of the coordinate

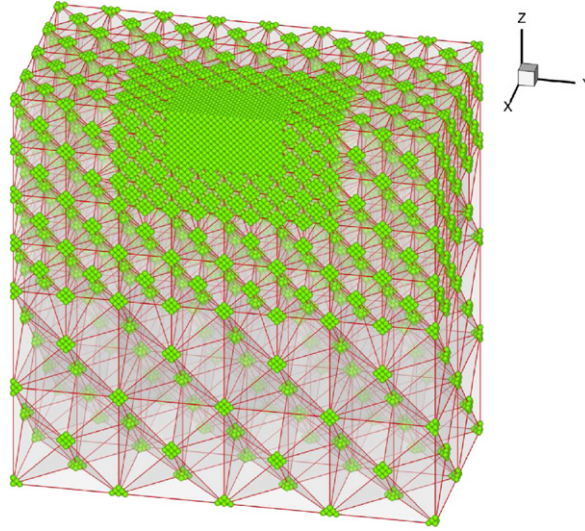


**Fig. 10.** Cross-section of the (001) oriented fcc single crystalline Al sample with initial triangulation and distribution of sampling atoms (green) for  $R_c = 1.0a_0$ .

system correspond to  $\langle 001 \rangle$  directions. A spherical indenter of radius  $R$  is modeled as an external potential  $V^{\text{ext}}$  of the form

$$V^{\text{ext}}(\mathbf{x}) = A \cdot \theta(R - r) \cdot (R - r)^3 \quad \text{with } r = |\mathbf{x} - \mathbf{c}|, \quad (36)$$

where parameter  $A$  represents the strength of the repulsive force,  $\theta(r)$  the step function,  $R$  the indenter radius and  $\mathbf{c}$  denotes the position of the midpoint of the indenter. In the simulations the values  $A = 2000 \text{ eV}/\text{\AA}^3$  and  $R = 16a_0$  with lattice constant  $a_0 = 4.032 \text{ \AA}$  are used. The energy of the crystal is modeled using the EAM potential of Ercolessi and Adams (1994). The ball indenter is driven into the [001] oriented single crystal in small displacement increments  $\Delta h$ , where at each loading step a new stable equilibrium configuration of the system is found by a nonlinear version of the CG method.

In order to make the simulations comparable, all details of the lattice statics simulation are maintained for the QC simulation: boundary conditions, modeling of the indenter, step size in the displacement controlled process and the extensions of the computational box.

The initial QC triangulation of the cubic computational box is specifically tailored to the nanoindentation geometry. Fig. 10 shows the initial distribution of representative atoms and the adjacent clusters of size  $R_c = 1.0a_0$ . In a small region of the crystal located directly underneath the indenter, fully atomistic resolution is chosen, which enables to resolve defect nucleation. With increasing distance to this region of interest the triangulation gradually becomes coarser. The initial discretization for  $R_c = 1.0a_0$  contains approx. 48 000 sampling atoms, which is less than 4.5% of the total number of atoms in the computational box.

A key issue in atomistic simulations in three dimensions is the identification and visualization of defects and microstructures. For that purpose indicators are necessary, that detect defects, allow to visually extract them from their undisturbed surroundings and to classify characteristic types of them, see e.g. Li (2005). Here we use the so-called *centro symmetry parameter*, introduced by Kelchner et al. (1998). The centro symmetry parameter is defined for each atom in an fcc crystal according to

$$P = \sum_{i=1}^6 |\mathbf{r}_i + \mathbf{r}_{-i}|^2, \quad (37)$$

where vectors  $\mathbf{r}_i$  and  $\mathbf{r}_{-i}$  correspond to the six pairs of next neighbors lying at opposite sites w.r.t. the considered atom in the lattice. By definition, the centro symmetry parameter is zero for an atom in the bulk of a perfect material subject to purely homogeneous elastic deformations. The deviation of  $P$  from zero therefore measures the strength of disturbed centro symmetry at a lattice site.

## 7.2. Surface effects

The very first step in the simulation is an initial relaxation, where no force of the indenter is present, such that the equilibrium configuration is mainly influenced by surface effects. It is a well-known fact, that the nonlocal QC generally suffers from a significant overestimate of surface effects, see e.g. the review paper of Miller and Tadmor (2002), which can

be best illustrated for a representative atom at the corner of a cubic specimen. Since a suchlike atom sees three surfaces, it generally will be a high-energy atom. If the considered corner rep-atom is part of a coarse-grained region, its cluster will represent a large volume and therefore its weighting factor  $n_i$  will be large. The resulting energy will be as though that entire volume of material is located close to free surfaces. This leads to a considerable overestimate of the energetic contribution of the corner and therefore to spurious relaxation of the specimen. A possible remedy is to choose fully atomistic resolution at free surfaces which is computationally expensive.

QC simulations of the initial relaxation are performed on the mesh in Fig. 10. The cluster radius is set to a relatively small value of  $R_c = 1.0a_0$  corresponding to 19 sampling atoms per cluster. In a second simulation  $R_c = 2\sqrt{2}a_0$  is chosen corresponding to 381 atoms per cluster. For comparison we perform the initial relaxation in a third calculation on the same mesh applying the force correction method as proposed in Section 6.2. Necessarily the two energy calculations are performed with cluster size  $R_c = a_0/\sqrt{2}$  and  $R_c^* = 2\sqrt{2}a_0$ . Fig. 11 displays the displacements in z-direction after the initial relaxation for both, lattice statics and the different QC-eFNL-simulations. As predicted by the introductory reasoning QC largely overestimates the shrinkage in z-direction for  $R_c = 1.0a_0$ , where the value at the corner of  $u_z = -3.3 \text{ \AA}$  is 2.5 times larger than that one of lattice statics,  $u_z = -1.3 \text{ \AA}$ . For  $R_c = 2\sqrt{2}a_0$  however,  $u_z = -1.1 \text{ \AA}$  is very close to the reference value of lattice statics. The same value of maximum shrinkage during relaxation is obtained by the hybrid force correction method, see Fig. 11. Hence, in this case QC-eFNL along with the two concepts for error control can accurately account for

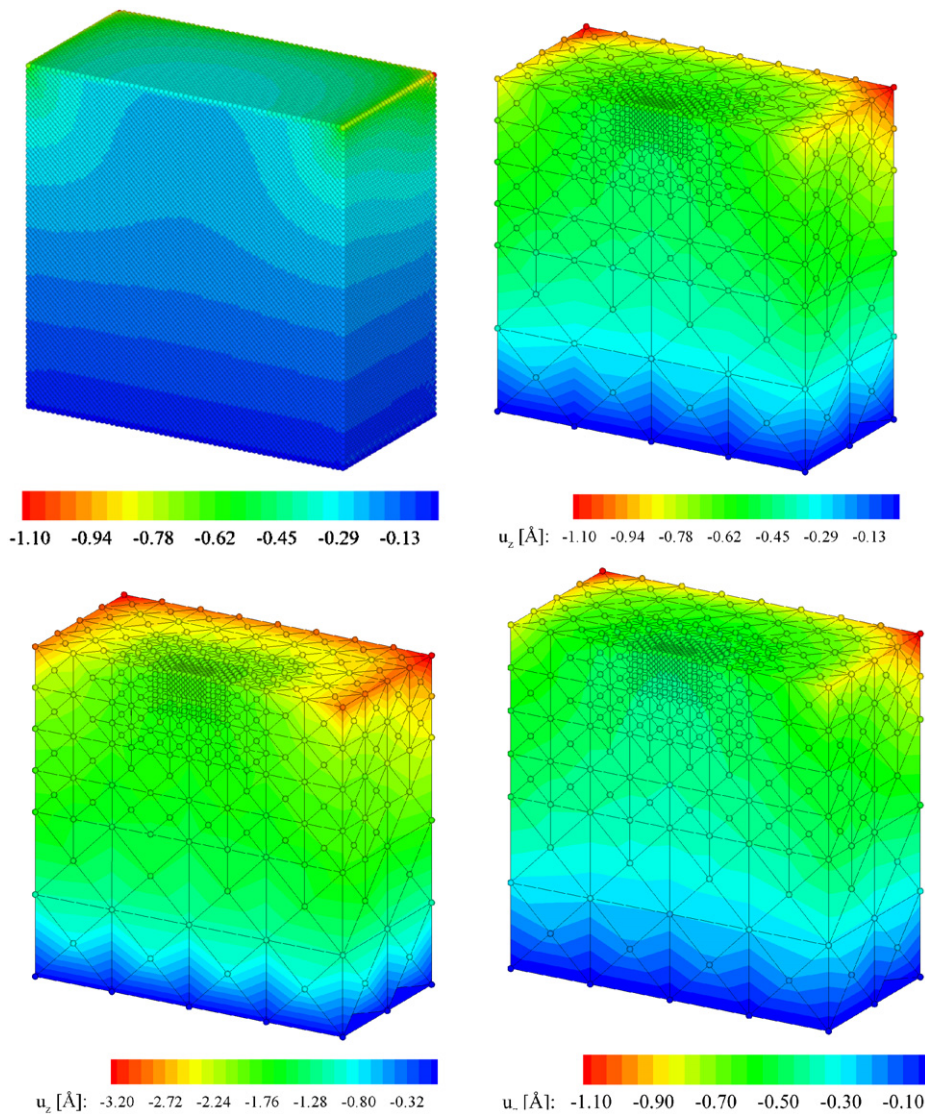


**Fig. 11.** Contours of displacements  $u_z$  [Å] after initial relaxation for (upper left) lattice statics:  $\min(u_z) = -1.3 \text{ \AA}$ , (upper right) QC-eFNL along with hybrid force correction,  $R_c = 1/\sqrt{2}a_0$ ,  $R_c^* = 2\sqrt{2}a_0$ :  $\min(u_z) = -1.1 \text{ \AA}$ , (bottom left) QC-eFNL,  $R_c = 1.0a_0$ :  $\min(u_z) = -3.3 \text{ \AA}$ , (bottom right)  $R_c = 2\sqrt{2}a_0$ :  $\min(u_z) = -1.1 \text{ \AA}$ .

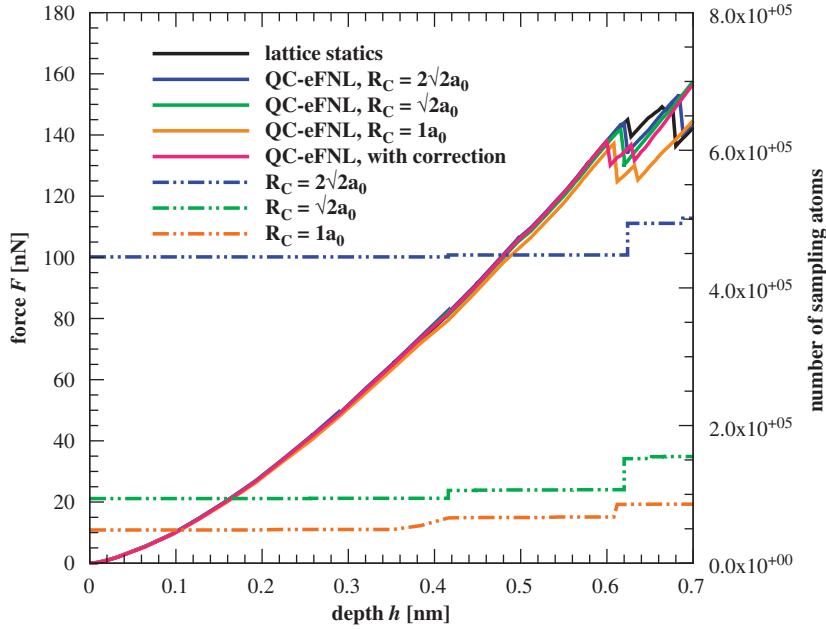


**Fig. 12.** Force–depth ( $F$ – $h$ ) curves for lattice statics and QC-eFNL simulations. The number of sampling atoms used in QC calculations is denoted by the dash-dotted lines.

surface effects even in coarse-grained regions, which effectively overcomes the necessity to choose a fine or even fully atomistic resolution in the vicinity of free surfaces.

### 7.3. Force–displacement curve and dislocation nucleation

During the deformation process the force–displacement curve is recorded, see Fig. 12. In the first branch of purely elastic deformation the force continuously increases. In this range, a large stepsize  $\Delta h \approx 0.3 \text{ \AA}$  is chosen. When a critical value of the indenter force  $F$  is reached, the first dislocation nucleates in the single crystal. This onset of plastic deformation is marked by a discrete force drop in the  $F$ – $h$  curve, see Fig. 12. In order to keep track of the evolving microstructure beneath the indenter, the step size is chosen to be much smaller,  $\Delta h = 0.02 \text{ \AA}$  for the subsequent loading steps.

In the elastic branch QC-eFNL generally well agrees with lattice statics. Increasing the cluster size to  $R_c = 2\sqrt{2}a_0$  already yields quantitative agreement between QC-eFNL and lattice statics. The application of static correction forces ( $R_c = a_0/\sqrt{2}$ ,  $R_c^* = 2\sqrt{2}a_0$ ) as outlined in Section 6 and already assessed for the initial relaxation step also results in perfect agreement of the  $F$ – $h$  curve with the reference solution.

The process of applying static correction forces is as follows. Two minimizations of the total energy are performed for each loading step; in the first run static forces of the former loading step are maintained, for the second relaxation run, static forces are newly calculated. The latter step implies, that the newly calculated correction forces—though formally derived from a correction potential—are no longer conservative.

Next, we consider dislocation nucleation beneath the indenter. The corresponding force drop in the  $F$ – $h$  curve occurs in the QC simulations for various cluster radii throughout at a somewhat smaller load level than for lattice statics. Increasing the cluster size improves the approximation, for  $R_c = 2\sqrt{2}a_0$  excellent agreement with the fully atomistic resolution is achieved, see Fig. 12.

The overall good agreement of QC-eFNL in the  $F$ – $h$  curve is a nice result, since the computational costs are tremendously reduced. For cluster radius  $R_c = 1.0a_0$  the number of sampling atoms increases during adaptive refinement steps from initially approx. 48 000 to approx. 86 000, which is still only 8 percent of the number of atoms used in the lattice statics simulation. The QC simulation for cluster radius  $R_c = 1.0a_0$  is approx. eight times faster than lattice statics, for  $R_c = 2\sqrt{2}a_0$  still two times faster. The efficiency can be arbitrarily improved by increasing the size of the simulation box, since only large elements are added in lateral and depth direction. Opposed to lattice statics we may now safely use large simulation boxes without great loss of efficiency to eliminate any undesirable simulation size effects.

Of course, the multiscale framework introduces some computational overhead such that problem sets of a critical size might be found where the multiscale simulations do not significantly reduce the computational burden of fully atomistic resolution. In cases however, where the problem characteristics dictate to simulate large systems without modeling reductions and simplifications as e.g. in systems with more complex geometries and/or boundary conditions, the extra

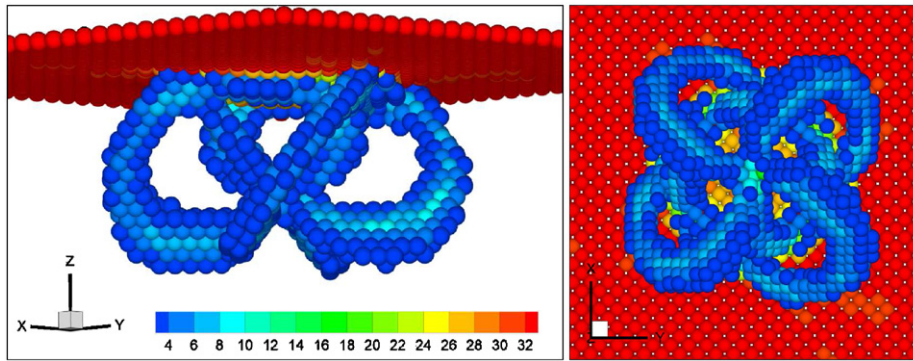


Fig. 13. Lattice statics simulation: dislocation microstructure visualized by centro symmetry parameter  $P \geq 2 \text{ \AA}^2$ .

multiscale effort will be overcompensated by the feature of atomic coarse-graining with adaptive resolution. In that case QC exhibits a gain in efficiency since it generally scales more favorable with system size than fully atomistic lattice statics.

#### 7.4. Dislocation microstructure

Fig. 13 displays the dislocation microstructure of lattice statics right after the second force drop in Fig. 12; four dislocation loops can be observed gliding on the family of  $\{111\}$  planes, i.e.  $(\bar{1}11)$ ,  $(1\bar{1}1)$ ,  $(11\bar{1})$  and  $(\bar{1}\bar{1}\bar{1})$ . In view of the directions of plastic slip on  $\{111\}$  planes, the nucleated dislocations are  $1/6[11\bar{2}](111)$  Shockley partials.

Among the QC simulations the type of microstructure agrees best with the one of lattice statics for cluster size  $R_c = 1.0a_0$ . Again, four dislocation loops are observed gliding on the family of  $\{111\}$  planes, see Fig. 14, first row. Simulations of higher accuracy by means of force correction or by a larger cluster size, exhibit some deviations in the evolving microstructure compared with lattice statics.

A possible explanation for this is that the QC method opposed to lattice statics generally exhibits a minimal asymmetry in the case of overlapping sampling clusters; sampling atoms, which have the same distance to more than one representative atom are randomly distributed to one of the representative atoms. Of course, this has a direct influence on the weighting factors of each representative atom. This means that even for a FE mesh of perfect symmetry the weighting factors may introduce a minimal asymmetry. Given this numerically induced asymmetry or any other slight numerical perturbation, the nonconvexity of the energy can lead to different results in terms of microstructures, cf. the results for a similar setup in Knap and Ortiz (2001). For that reason a one-to-one correspondence of the dislocation structures is generally questionable on fundamental grounds and cannot be expected.

## 8. Summary and conclusion

We have presented a novel version of a fully nonlocal, 3D quasicontinuum (QC) method, which is inspired by the seminal work of Knap and Ortiz (2001).

- (I) Conceptually the novel QC formulation based on energy sampling, QC-eFNL, exhibits advantages compared to its precursor:
  - (1) Sampling at the energy level instead of the force level preserves the variational structure of lattice statics in the fully nonlocal QC method leading to conservative forces, Eq. (24), and to symmetric stiffness matrices, Eq. (25).
  - (2) More specifically, energy sampling implies the strict symmetry of atomic interactions in all regions, even across the boundary of clusters, whereas force sampling does not.
  - (3) Numerical advantages follow from theoretical consistency:
    - (a) Standard algorithms for the numerical minimization of functionals like CG methods can directly be applied, since they generally require gradients as well as evaluations of the functional itself.
    - (b) A minimizer can be found, if the energy exhibits a minimum.
    - (c) For the widely used EAM potentials the present energy-based sampling method requires the consideration of less kinematically constrained atoms to calculate the electron density, cf. Eqs. (26) and (27).
    - (d) The stability of the crystal can be assessed by the eigenvalues of the symmetric stiffness matrix, where an artificial asymmetry may falsify this analysis.
- (II) An error analysis has elucidated the quality and has assessed the quantity of error in QC-eFNL, which results in the proposal of a novel strategy for error control.

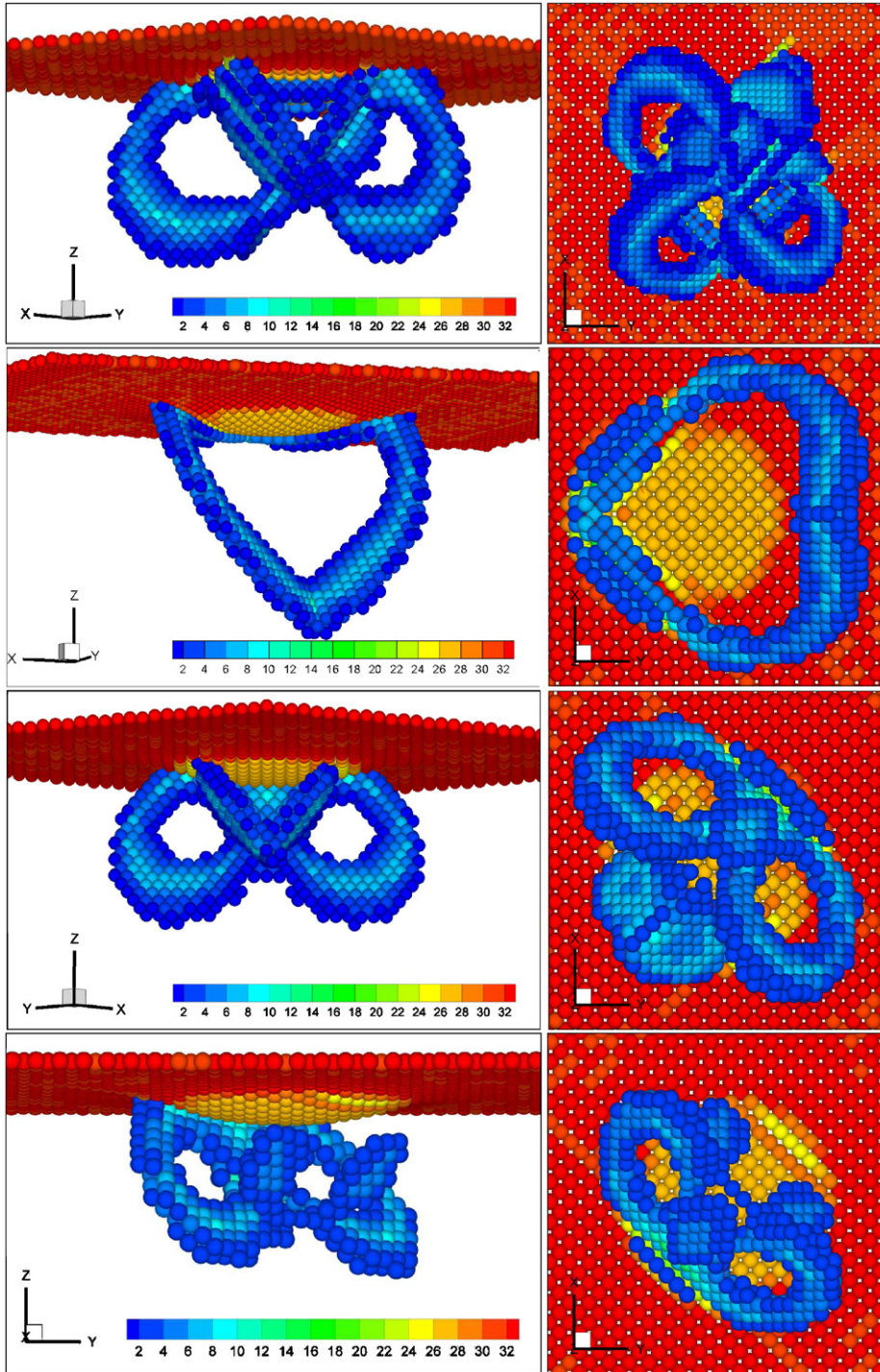


**Fig. 14.** QC-eFNL simulations: dislocation microstructure visualized by centro symmetry parameter  $P \geq 2 \text{ \AA}^2$ . Rows 1–3: simulations for  $R_c = 1.0a_0; \sqrt{2}a_0; 2\sqrt{2}a_0$ . Row 4: simulation with hybrid force correction applied.

- (4) For residual forces observed in QC-eFNL simulations, the following properties have been shown. Residual forces are conservative in nature; they do not follow from an asymmetry in atomic interactions as a consequence of inconsistent a priori assumptions on how atoms interact; they stem from the error in numerical quadrature and therefore can be reduced (to identically zero) by a sufficiently large cluster size. As such, the present residual forces differ from ghost forces in QC-CBR by source and property, which is the reason why we distinguish by name.

- (5) For error control a hybrid method based on static corrective forces has been proposed which is more efficient than increasing the sampling cluster size. Although these forces are derived from a correction potential, they are no longer conservative, if they are recalculated for an update in a sequence of loading steps. It is shown that both methods of error control enable QC-eFNL to accurately account for surface effects in the case of nanoindentation even in coarse-grained surface regions. In order to obtain a definite statement on the method's capacity to precisely capture surface effects in e.g. largely strained nanostructures like nanowires, an additional comprehensive analysis is necessary.
- (III) The simulation of nanoindentation into an (001) fcc single crystal has proved the overall efficiency of the method's coarse-graining with adaptive resolution. Compared with lattice statics, the  $F$ - $h$  curve as well as the load level of dislocation nucleation can be quantitatively captured by a proper choice of the sampling cluster size. The observed dislocation microstructures vary in some details, but generally well agree with the result of fully atomistic resolution.

Briefly, the simulations have shown the promising capacity of QC-eFNL to reduce the prohibitive computational expense of fully atomistic resolution while faithfully simulating the material's response in significant details.

## References

- Brenner, S.C., Scott, L.R., 2002. *The Mathematical Theory of Finite Element Methods*. Springer, New York.
- Cheng, Y.T., Page, T., Pharr, G.M., Swain, M.V., Wahl, K.J., 2004 (Guest Eds.), *Fundamentals and applications of instrumented indentation in multidisciplinary research*. *J. Mater. Res.* 19, 1–395.
- Curtin, W.A., Miller, R.E., 2003. Atomistic/continuum coupling in computational materials science. *Modelling Simul. Mater. Sci. Eng.* 11 (3), R33–R68.
- Daw, M.S., Baskes, M.L., 1984. Embedded-atom method: derivation and application to impurities, surfaces, and other defects in metals. *Phys. Rev. B* 29 (12), 6443–6453.
- E, W., Lu, J., Yang, J.Z., 2006. Uniform accuracy of the quasicontinuum method. *Phys. Rev. B* 74 (12), 214115.
- Ercolessi, F., Adams, J.B., 1994. Interatomic potentials from first-principles calculations: the force-matching method. *Europhys. Lett.* 26, 583–588.
- Gerberich, W.W., Nelson, J.C., Lilleodden, E.T., Anderson, P., Wyrobek, J.T., 1996. Indentation induced dislocation nucleation: the initial yield point. *Acta Mater.* 44 (9), 3585–3598.
- Gouldstone, A., Chollacoop, N., Dao, M., Li, J., Minor, A.M., Shen, Y.L., 2007. Indentation across size scales and disciplines: recent developments in experimentation and modeling. *Acta Mater.* 55, 4015–4039.
- Hayes, R.L., Fago, M., Ortiz, M., Carter, E.A., 2005. Prediction of dislocation nucleation during nanoindentation by the orbital-free density functional theory local quasi-continuum method. *Multiscale Model. Sim.* 4 (2), 359–389.
- Hughes, T.J.R., 2000. *Linear Static and Dynamic Finite Element Method*. Dover Publications, Mineola.
- Kelchner, C.L., Plimpton, S.J., Hamilton, J.C., 1998. Dislocation nucleation and defect structure during surface indentation. *Phys. Rev. B* 58 (4), 11085.
- Knap, J., Ortiz, M., 2001. An analysis of the quasicontinuum method. *J. Mech. Phys. Solids* 49, 1899–1923.
- Knap, J., Ortiz, M., 2003. Effect of indenter-radius size on Au (001) nanoindentation. *Phys. Rev. Lett.* 90 (4), 226102.
- Kohlhoff, S., Gumbsch, P., Fischmeister, H.F., 1991. Crack propagation in bcc crystals studied with a combined finite-element and atomistic model. *Philos. Mag.* A 64, 851–878.
- Kulkarni, Y., Knap, J., Ortiz, M., 2008. A variational approach to coarse-graining of equilibrium and non-equilibrium atomistic description at finite temperature. *J. Mech. Phys. Solids* 56, 1417–1449.
- Lennard-Jones, 1924. On the determination of molecular fields. II. From the equation of state of a gas. *Proc. R. Soc. London* 106A, 463.
- Li, J., 2005. Atomistic visualization. In: Yip, S. (Ed.), *Handbook of Materials Modeling*. Springer, Dordrecht, pp. 1051–1068.
- Luenberger, D.G., 1989. *Linear and Nonlinear Programming*. Addison-Wesley, Reading.
- Marian, J., Knap, J., Ortiz, M., 2004. Nanovoid cavitation by dislocation emission in aluminum. *Phys. Rev. Lett.* 93 (4), 165503.
- Miller, R.E., Tadmor, E.B., 2002. The quasicontinuum method: overview, applications and current directions. *J. Comput. Aided Mater. Des.* 9 (3), 203–239.
- Miller, R., Ortiz, M., Phillips, R., Shenoy, V., Tadmor, E.B., 1998a. Quasicontinuum models of fracture and plasticity. *Eng. Fract. Mech.* 61 (3–4), 427–444.
- Miller, R., Tadmor, E.B., Phillips, R., Ortiz, M., 1998b. Quasicontinuum simulation of fracture at the atomic scale. *Modelling Simul. Mater. Sci. Eng.* 6, 607–638.
- Minor, A.M., Asif, S.A.S., Shan, Z., Stach, E.A., Cyranowski, E., Wyrobek, T.J., Warren, O.L., 2006. A new view of the onset of plasticity during the nanoindentation of aluminum. *Nature Mater.* 5, 697–702.
- Mullins, M., Dokainish, M.A., 1982. Simulation of the (001) plane crack of  $\alpha$ -iron employing a new boundary scheme. *Philos. Mag.* A 46, 771–787.
- Phillips, R., Rodney, D., Shenoy, V., Tadmor, E.B., Ortiz, M., 1999. Hierarchical models of plasticity: dislocation nucleation and interaction. *Modelling Simul. Mater. Sci. Eng.* 7, 769–780.
- Picu, R.C., 2000. Atomistic-continuum simulation of nano-indentation in molybdenum. *J. Comput.-Aided Mater. Des.* 7 (2), 77–87.
- Rodríguez de la Fuente, O., Zimmerman, J.A., González, M.A., Figuera de la, J., Hamilton, J.C., Pai, W.W., Rojo, J.M., 2002. Dislocation emission around nanoindentations on a (001) fcc metal surface studied by scanning tunneling microscopy and atomistic simulations. *Phys. Rev. Lett.* 88 (4), 036101.
- Sansoz, F., Molinari, J.F., 2005. Mechanical behavior of  $\Sigma$  tilt grain boundaries in nanoscale Cu and Al: a quasicontinuum study. *Acta Mater.* 53 (7), 1931–1944.
- Saraev, D., Miller, R.E., 2005. Atomistic simulation of nanoindentation into copper multilayers. *Modelling Simul. Mater. Sci. Eng.* 13 (7), 1089–1099.
- Shenoy, V.B., Miller, R., Tadmor, E.B., Rodney, D., Phillips, R., Ortiz, M., 1999. An adaptive finite element approach to atomic-scale mechanics—the quasicontinuum method. *J. Mech. Phys. Solids* 47, 611–642.
- Shenoy, V.B., Phillips, R., Tadmor, E.B., 2000. Nucleation of dislocations beneath a plane strain indenter. *J. Mech. Phys. Solids* 48, 649–673.
- Shewchuk, J.R., 1994. An introduction to the conjugate gradient method without the agonizing pain. URL: (<http://www.cs.cmu.edu/~jrs/jrspapers.html#cg>).
- Shimokawa, T., Mortensen, J.J., Schiøtz, J., Jacobsen, K.W., 2004. Matching conditions in the quasicontinuum method: removal of the error introduced at the interface between the coarse-grained and fully atomistic region. *Phys. Rev. B* 69 (10), 214104.
- Smith, G.S., Tadmor, E.B., Kaxiras, E., 2000. Multiscale simulation of loading and electrical resistance in silicon nanoindentation. *Phys. Rev. Lett.* 84 (4), 1260.
- Smith, G.S., Tadmor, E.B., Bernstein, N., Kaxiras, E., 2001. Multiscale simulations of silicon nanoindentation. *Acta Mater.* 49, 4089–4101.
- Tadmor, E.B., Phillips, R., Ortiz, M., 1996a. Mixed atomistic and continuum models of deformation in solids. *Langmuir* 12 (19), 4529–4534.
- Tadmor, E.B., Ortiz, M., Phillips, R., 1996b. Quasicontinuum analysis of defects in solids. *Philos. Mag.* 73, 1529–1563.
- Tadmor, E.B., Miller, R., Phillips, R., Ortiz, M., 1999. Nanoindentation and incipient plasticity. *J. Mater. Res.* 14 (6), 2233–2250.
- Wallace, D.C., 1998. *Thermodynamics of Crystals*. Dover Publications, Mineola.